Impact of recycling and lateral sediment input on grain size fining trends – implications for reconstructing tectonic and climate forcings in ancient sedimentary systems

Impact of recycling and lateral sediment input on grain size fining trends – implications for reconstructing tectonic and climate forcings in ancient sedimentary systems

Rebekah Harries*[1], L. A. Kirstein[1], A. Whittaker[2], M. Attal[1], Ian Main[1]

[1]The University of Edinburgh, [2]Imperial College London

*Corresponding author email: rebekah.m.harries@gmail.com

Abstract

Grain size trends in basin stratigraphy are thought to preserve a rich record of the climatic and tectonic controls on landscape evolution. Stratigraphic models assume that over geological timescales, the downstream profile of sediment deposition is in dynamic equilibrium with the spatial distribution of tectonic subsidence in the basin, sea level and the flux and calibre of sediment supplied from mountain catchments. Here we demonstrate that this approach to modelling stratigraphic responses to environmental change is missing a key ingredient: the dynamic geomorphology of the sediment routing system. For three large alluvial fans in the Iglesia basin, Argentine Andes we measured the grain size of modern river sediment from fan apex to toe and characterise the spatial distribution of differential subsidence for each fan by constructing a 3D model of basin stratigraphy from seismic data. We find, using a self-similar grain size fining model, that the profile of grain size fining on all three fans cannot be reproduced given the subsidence profile measured and for any sediment supply scenario. However, by adapting the self-similar model, we demonstrate that the grain size trends on each fan can be effectively reproduced when sediment is not only sourced from a single catchment at the apex of the system, but also laterally, from tributary catchments and through fan surface recycling. Without constraint on the dynamic geomorphology of these large alluvial systems, signals of tectonic and climate forcing in grain size data are masked and would be indecipherable in the geological record. This has significant implications for our ability to make sensitive, quantitative reconstructions of external boundary conditions from the sedimentary record.

1. Introduction

1.1. Rationale

The grain size and rate of fining downstream of alluvial sediment are key physical attributes that can store important environmental information (Heller & Paola, 1992; Robinson & Slingerland, 1998; Hoey & Bluck, 1999; Duller *et al.*, 2010). Climatic and tectonic boundary conditions are documented to control the volume and calibre of sediment released into depositional basins (Hovius & Leeder, 1998; Allen *et al.*, 2017; Roda-Boluda & Whittaker, 2018). This sediment is then deposited downstream at a rate controlled both by the spatial distribution of tectonic subsidence and the dynamics of sediment transport and deposition (Fedele & Paola, 2007; Duller *et al.*, 2010; Whittaker *et al.*, 2011). Quantitative inversions of downstream grain size trends for the rate of sediment supply and accommodation generation could therefore provide a window into the climatic and tectonic settings of the past (e.g. Duller *et al.*, 2010; Allen *et al.*, 2013) with recent studies linking changing grain size fining rate in alluvial fan settings to both tectonic and environmental drivers (e.g. Parsons *et al.*, 2012; D'Arcy *et al.*, 2017). However, numerical models and flume experiments have shown that dynamic fluctuations in bed surface morphology over geomorphic timescales can buffer the transfer of an environmental signal into depositional stratigraphy (Humphrey & Heller, 1995; Jerolmack & Paola, 2010), even where input sediment fluxes from upland catchments can be linked to changing climate (Waters *et al.*, 2010; McPhillips *et al.*, 2013; D'Arcy *et al.*, 2017). Moreover, while numerical models of sediment routing systems are capable of producing convincing stratigraphic patterns (Allen & Densmore, 2000; Armitage *et al.*, 2011; Allen & Heller, 2012; Forzoni *et al.*, 2014), they often fail to consider how sediment recycling and multiple sediment inputs influence the mass balance of the system and the distribution of grain sizes in a basin over geologically meaningful timescales (Rice, 1998; Malatesta *et al.*, 2017; Malatesta *et al.*, 2018). A better understanding of this problem is crucial to characterise the sensitivity of the fluvial systems at the Earth's surface to changing tectono-climatic boundary conditions over a range of spatial and temporal scales (Pelletier *et al.*, 2015; Romans *et al.*, 2016).

For fluvial systems transporting abrasion-resistant clasts as bedload, classical models solving the downstream distribution of grain sizes on a river bed emulate the hydraulically driven, size selectivity of sediment transport processes that are well-documented in laboratory flume experiments (e.g. Parker, 1991a; Paola & Seal, 1995; Hoey & Ferguson, 1997). For instance, a poorly sorted sediment load, fed to the apex of the flume, will fractionate downstream due to the preferential deposition of coarser clasts, at a rate controlled by the rivers transport capacity and its sediment supply (Paola *et al.*, 1992; Seal *et al.*, 1997). However, in natural systems, tributaries, hillslopes and the recycling of fluvial terraces introduce significant additional sources of sediment laterally into the system, so that the downstream fractionation of grain sizes integrates both local and downstream sediment supplies (Pizzuto, 1995; Rice, 1998; Rice & Church, 1998; Rice, 1999). The processing of lateral inputs of sediment has been highlighted as a potential buffer for the translation of environmental signals into stratigraphy and is a major source of uncertainty in numerical models of sediment routing systems (Rice & Church, 1998; Jerolmack & Paola, 2010; Allen *et al.*, 2017; Malatesta *et al.*, 2017). To-date a number of field observations report lateral sediment inputs having variable impacts on downstream fining trends (Church & Kellerhals, 1978; Constantine *et al.*, 2003). There is evidence in some rivers for lateral inputs redefining the particle size distribution along the main river channel (Rice, 1998; Rice & Church, 1998; Constantine *et al.*, 2003; Attal & Lavé, 2006; Whittaker *et al.*, 2010; Attal *et al.*, 2015). Rice (1999) developed the term 'sedimentary links' to describe longitudinal sections of river, between tributary confluences, which have distinctly different rates of downstream fining. In other cases, a consistent rate of downstream fining is preserved along the river and there is little evidence of lateral sediment inputs having any persistent impact on surface size distributions (Hoey & Bluck, 1999; Gomez *et al.*, 2001; Singer, 2008). Ferguson *et al.* (2006) demonstrate that the interplay between water discharge, sediment flux and sediment size at tributary confluences impact the river's long profile and local grain size variability. Whether lateral inputs disrupt, perturb or have no influence on grain size fining trends has been tied to disparity between the relative volumes and grain sizes of the mixing loads and is likely a function of the degree of sorting of the lateral input supply during transport

between sediment source region and confluence (Singer, 2008). In this paper, we evaluate the impact lateral inputs of sediment have on grain size fining in Holocene streamflow-dominated gravel deposits by using alluvial fans in the Iglesia basin as a case study to assess the impact of multiple sediment inputs in modulating grain size fining where basin subsidence rates and source catchment sediment fluxes can be constrained independently. We use this data to evaluate the circumstances in which sediment recycling impedes the extraction of tectono-climatic signals from grain size fining trends from Holocene depositional systems.

1.2. Approach

Probabilistic modelling of down-system grain size fining patterns as sediment is supplied laterally and moved axially requires knowledge of a large number of hydraulic variables to constrain the grain scale processes controlling bedload mixing and deposition along a channel reach (Parker, 1991b; Paola & Seal, 1995; Hoey & Ferguson, 1997; Robinson & Slingerland, 1998; Wilcock & Kenworthy, 2002). In making several simplifying assumptions, Ferguson et al. (2006) applied a 1D numerical model to investigate the impact of a tributary on the width-averaged bed elevation and grain size distribution along a channel profile. This approach recognised the complex evolution of sediment flux, water discharge and bedload diameter ratios between the mainstream and a tributary and their impact on channel aggradation or degradation and grain size along the river. However, it is also recognised that the rate of downstream grain size fining often scales, to a first order, with the size of the depositional system (Hoey & Bluck, 1999), indicating that transient fluctuations in a river's bed surface have limited impact on their grain size profiles. Fedele and Paola (2007) offered a deterministic solution for downstream grain size fining that simplifies the complexities of sediment transport over large temporal and spatial scales. Their solution is based on observations from numerical models and flume experiments that find aggrading rivers that reach near steady state develop self-similar substrate size distributions along substrate fining profiles that are positively correlated with self-similar bed profiles.

Fedele and Paola (2007) tie this self-organising behaviour to the well documented mechanism by which channels modify their morphology in order to maintain a dimensionless shear stress slightly above the critical Shields stress required for incipient motion (Shields, 1936; Parker, 1978; Buffington & Montgomery, 1997; Mueller *et al.*, 2005; Lamb *et al.*, 2008). A constant value of the critical Shields stress is often used to scale bedload sediment transport in numerical models (e.g. Meyer-Peter & Muller, 1948). By invoking a constant Shields stress, specific to a bedload regime for gravel transport, Fedele and Paola (2007) are able to characterise the relative mobility of clast sizes from an inversion of the self-similar size distribution of clasts on the bed surface. They define their relative mobility function as $J_i = p_i/F_i$ where p_i represents the proportion of the ith grain size fraction in transport and F_i, is the proportion of that fraction in the bed surface(c.f. Paola & Seal, 1995). More detail on J_i is provided in the appendix. The partitioning of variance in the sediment supply between local variability at a sample site and the variance in the downstream direction, which manifests as downstream fining, can therefore be solved analytically using J_i and the wider mass balance of the sediment routing system.

The starting point for Fedele and Paola's (2007) solution for downstream grain size fining describes sediment deposition using a fractional Exner sediment mass balance:

$$\left(1-\lambda_p\right)\left(r_{\delta t}(X)+\frac{\delta\eta}{\delta t}(X)\right)=-\frac{\delta q_s}{\delta X} \qquad \text{Equation 1}$$

where the rate of change in sediment discharge with downstream distance, $\delta q_s/\delta X$, is a function of the longitudinal spatial distribution of tectonic subsidence over time, $r_{\delta t}(X)$, the rate of change in bed elevation at a given downstream distance, $\delta\eta/\delta t\ (X)$, and sediment porosity, λ_p. This equation can be rearranged to construct a 2D horizontal profile of mass extraction from an initial sediment flux, q_{s0} , along the total length, L, of a depositional system:

$$q_s(X)=\ q_{s0}\ -\left(1-\ \lambda_p\right)\int_0^L r_{\delta t}(X)dX \qquad \text{Equation 2}$$

Fedele and Paola (2007) show that the fraction of a given sediment size deposited, f, from a transported load at any dimensionless downstream distance x^*, where $x^* = X/L$, can be solved for any distribution of mass deposited down-system, R^* :

$$R^*(x^*) = \left(1 - \lambda_p\right) L \frac{r^*(x^*)}{q_s(x^*)} \qquad \textit{Equation 3}$$

Assuming geomorphic fluctuations in the bed surface are transient over long timescales, R^* is a ratio of the space made available for deposition by tectonic subsidence, $r^*(x^*)$, and the flux of sediment supplied to fill the space, $q_s(x^*)$. In such cases, the distribution of sediment extraction is described by a simple mass conserving sorting process and can be solved:

$$\frac{df}{dx^*} = f\left[R^*\left(1 - \frac{1}{J_i}\right) - \frac{1}{J_i}\frac{dJ_i}{dx^*}\right] \qquad \text{Equation 4}$$

Although not specifically addressed by Fedele and Paola (2007) and subsequent authors (e.g. Duller *et al.*, 2010), this approach sets up a mass balance framework that would in principle allow us to treat the mixing of lateral inputs with trunk stream inputs as function of their relative fluxes and grain size distributions. We are able to vary $q_s(x^*)$ as a discontinuous function of x^*. It is therefore a powerful tool that can be used to better understand how lateral inputs of sediment might impact the downstream fining of grain sizes in a sediment routing system over stratigraphic timescales.

In this paper, we apply Fedele and Paola's (2007) 2D self-similar solution for downstream grain size fining to field data collected from three large, arid alluvial fans in the Iglesia basin, south central Argentine Andes. We exploit the Fedele and Paola (2007) model to examine the impact of sediment recycling and tributaries on downstream grain size fining trends on alluvial fans. In particular we adapt the mass balance framework within the model to account for lateral inputs from both tributary and recycled terrace sources.

2. Study Area

The Iglesia basin is a wedge-top, piggyback basin, separating the Frontal Cordillera of the Argentine Andes on the west, from a thin-skinned, Precordillera fold and thrust belt to the east (Allmendinger *et al.*, 1990; Suriano *et al.*, 2015) (figure 1). These structures accommodated compression from the shallow subduction of the Nazca plate throughout the Neogene and translated the Iglesia basin passively on top of the westernmost thrust sheet (Alvarez-Marron *et al.*, 2006). The tectonic, climatic and base level controls on the evolution of the Iglesia basin have received much attention due to the large amount of data available on the basin's stratigraphy. We use these data, outlined below, to constrain the distribution of accommodation within the basin at high resolution.

A 48-channel active-source reflection seismic survey, sampling the majority of the basin's longitudinal axis, was carried out in 1980-1981 by Argentine oil company Yacimientos Petroliferos Fiscales. These data have been analysed by several authors (Snyder, 1988; Beer *et al.*, 1990; Fernández-Seveso, 1993; Ruskin & Jordan, 2007). The shape of the basin is controlled by tectonic movement on the basins margins as well as on intrabasinal thrusts associated with the El Tigre strike-slip deformation zone (Allmendinger *et al.*, 1990). In the centre of the basin, the fill is ~3.5 km thick. To the west, strata decrease in thickness and onlap onto a basement surface that dips 12^{o} east (Allmendinger *et al.*, 1990; Ruskin & Jordan, 2007). Allmendinger *et al.* (1990) observe that although there is a change in slope between the Frontal Cordillera and the basin, there is no surface-breaking thrust, suggesting the Frontal Cordillera uplifted as a growing fault-bend anticline over a buried ramp, effectively tilting the basin to the east. In the east of the basin, fault-propagation folds associated with intrabasinal thrusts at depth, have exposed the entirety of the basin fill in surface outcrops (Ruskin & Jordan, 2007). Alvarez-Marron *et al.* (2006) interprets the large-scale architecture of these out-of-sequence thrusts as a positive flower structure, where Miocene and Pliocene sedimentation was synchronous with faulting. Ruskin and Jordan (2007) identify eleven sequence boundaries within the basin's fill, as shown in the representative cross section presented in figure 2, taken from Ruskin (2006). They find

168 seismic sequences are physically continuous with the strata exposed, allowing for a multiproxy
169 analysis of the sediments in sequence and for good age constraints on sequence deposition, using
170 magnetostratigraphic and radiometric dating techniques. All but the lowest sequence (1 in figure 2)
171 were deposited between 9 Ma and 4.3 Ma (Jordan *et al.*, 1997; Re *et al.*, 2003) and sequences younger
172 than ~7 Ma were restricted to the west of the intrabasinal fault zone, highlighted in figure 2, as the
173 basin narrowed. Younger strata, deposited in the basin, likely during a period of internal drainage,
174 were evacuated to the Bermejo foreland < 2 Ma, as a through-going drainage system across the
175 Precordillera was established (Val *et al.*, 2016). Today, four generations of alluvial fan terraces overlie
176 a levelled Neogene surface in the proximal-medial piedmont (Perucca & Martos, 2012; Val *et al.*,
177 2016). The alluvial terraces increase in thickness basin-wards, where Perucca and Martos (2012)
178 report Quaternary sediments 0.1-3 m thick in the proximal-medial piedmont, thickening to 10 m in
179 the distal piedmont. Continued uplift of the proximal piedmont is thought to have isolated the oldest
180 exposed fan terrace (Perucca & Martos, 2012). These Iglesia basin terraces have not been dated,
181 though Perucca and Martos (2012) suggest their chronology can be correlated with alluvial surfaces
182 dated by Siame *et al.* (1997) on the eastern piedmont further south. Siame *et al.* (1997) provide
183 cosmogenic dates for an oldest surface of ~ 770 kyr, where the youngest surface is ~ 40 kyr. There is
184 no evidence for a significant change in uplift of the Frontal Cordillera through the Quaternary,
185 therefore the structure of the basin is assumed stable up to present with only minor neotectonic
186 faulting affecting mid-Quaternary surfaces in the east of the basin (Perucca & Martos, 2012).

187 Accumulation rates in the basin likely varied over time as sediment export to the foredeep occurred
188 intermittently with the opening and closure of a through-going drainage system across the
189 Precordillera (Suriano *et al.*, 2015). From ^{10}Be cosmogenic concentrations in sediments sampled
190 upstream of the Iglesia basin, Val *et al.* (2016) derive paleo-erosion rates of ~ 0.1-0.25 mm/yr between
191 7 and 5.2 Ma. These erosion rates are comparable to accumulation rates derived by Ruskin (2006)
192 from magnetostratigraphy, where a marked decrease in accumulation from >10 m / 10kyr in the late
193 Miocene uplift phase, to 0.1- 1 m / 10kyr in the Pliocene is observed. These latter rates are comparable

to regional millennial scale erosion rates for the Holocene (Bookhagen & Strecker, 2012; Carretier *et al.*, 2015).

Sediment transport events in the Iglesia basin today occur during infrequent summer storms linked to meteorological variations of the El Niño Southern Oscillation (ENSO), which drives irregular distributions of intense rainfall over the region. The impact of ENSO variability is evident in the Holocene sedimentary record of the Jachal River valley (Colombo et al., 2000; 2009) and over prints lower amplitude fluctuations in aridity (Iriondo and Garcia, 1993). During these short-lived events, sediment transport on the Iglesia fans occurs via channelized flow (Perucca & Martos, 2012) within an unarmoured bed (Harries *et al.*, 2018).

In this study, we focus on three catchment-alluvial fans on the Frontal Cordillera margin of the Iglesia basin (figure 1). These fans are excellent candidates for investigating size-selective transport in natural alluvial systems for several reasons: firstly, gravel transported on these fans is lithologically-hard, potentially limiting the impact of clast abrasion on the gravel mass balance of the systems. The gravel is a mix of predominantly intrusive, extrusive and sedimentary rocks sourced from the Andean Frontal Cordillera, generally transported by stream-bed flow for up to 40 km from the mountain front. Typical abrasion rates for gravel essentially made of intrusive and extrusive rocks are < 1 % mass-loss / km, equivalent to a fining rate ≤ 0.3 % / km, but we note that rates for sedimentary rocks may vary over orders of magnitude (Attal *et al.*, 2006; Attal & Lavé, 2009). We work here with the assumption that abrasion has a minimal influence on the grain size trends along the fans and later discuss this assumption in light of our data. Furthermore, these systems have not been heavily modified by human activity and the semi-arid climate means vegetation cover is minimal, eliminating an additional control on sediment transport that might otherwise influence grain size trends along the rivers.

The largest of the three fans, ~40 km in downstream length, is named fan 1 and drains into the centre of the basin. Two smaller fans, 2 and 3, are ~25 km in downstream length, are located south and north of fan 1, respectively. Each fan is fed by a primary catchment and between two and four tributary catchments of variable sizes (see also *Harries et al*., 2018). Smaller tributary catchments that feed directly into the mainstream, introduce sediment in the uppermost reaches of the fan, while larger tributary catchments have confluences with the main channel up to half way down fan, with sediment transport distances comparable to that in the trunk stream. The river channels are incised $\leq$2 m along their length into a fan surface attributed to the early Holocene (Perucca & Martos, 2012), where the modern channels themselves are braided with a channel and gravel bar morphology (*Harries et al*., 2018).

3. Methods

We investigate the extent to which Holocene downstream grain size fining trends on three adjacent catchment-alluvial fan systems in the Iglesia basin reflect the predictions of extant grain size fining models (e.g. Fedele & Paola, 2007; Duller *et al.*, 2010). We evaluate whether the external boundary conditions of each system can be reliably reconstructed from quantitative inversions of their Holocene downstream grain size fining trends and rates and patterns of subsidence. Here, we use the term subsidence to denote the differential subsidence generated by plate flexure due to loading and tectonic uplift, which together control the spatial distribution of accommodation space in the basin.

Gravel size data collected along the three alluvial fans are used to characterise the profile of grain size fining from fan apex to toe (section 3.1). A 3D model of basin stratigraphy is developed for the Iglesia basin through the mapping of sequence boundaries, imaged in seismic data (section 3.2). This is used to constrain the spatial distribution of sediment extraction, which is required as a parameter in the *Fedele and Paola* (2007) self-similarity grain size fining model; from this we compare the modelled downstream distribution of gravel grain sizes compared to the fining profile measured in the field

241 (section 3.3). Finally, we adapt this fining model to incorporate lateral inputs from both tributaries and
242 terrace recycling (section 3.4).

243 ### *3.1 Field data – Grain size*

244 Surface grain size distributions were measured on the alluvial fans in October 2015 and are also
245 presented in *Harries et al.* (2018), where the self-similarity in these grain size distributions is reported.
246 In this contribution, we instead focus on the controls on downstream fining in these deposits. These
247 data were collected at ~3 km intervals along the length of each alluvial river traversing the three fans,
248 where measurements were spaced so to avoid sampling within 1.5 km of tributary confluences (figure
249 1). At each locality we measured the size distribution of gravel (> 2mm) exposed on the dry, riverbed
250 surface, the depth of channel incision and recorded the lithology of each clast sampled (figure A1).
251 We assume that sediment finer than 2 mm (i.e. sand) is not transported as bedload and omit the finer
252 size fractions from our analysis. An analysis of the clast lithology data is presented in the Appendix.
253 The size distribution of gravel was characterised from the point counting of 200 clasts from two
254 photographs; where 100 clasts were sampled from each photograph using an equally spaced grid
255 (spacing ~200 mm) to systematically select clasts (c.f. Attal & Lavé, 2006; Whittaker *et al.*, 2011; Dingle
256 *et al.*, 2016). To account for the greater volumetric significance of larger clasts on the bed, we counted
257 clasts that cover *n* grid nodes *n* times in line with Kellerhals and Bray (1971) and previous publications
258 in this field (Whittaker *et al.*, 2011; D'Arcy *et al.*, 2017). To attain a sample that was spatially
259 representative of each locality, bar and channel deposits were sampled individually and their size
260 distributions subsequently merged into a single composite distribution (c.f. Bunte & Abt, 2001). The
261 bars present were both medial and alternating channel bars. Patchiness in grain size within these
262 structures was subtle and less prominent than the grain size variance between sites. The relative
263 contributions of gravel bar and channel deposits at each site were scaled by in-situ field estimates of
264 their relative percentage cover on the bed (c.f. Bunte & Abt, 2001).

An analysis of the precision and potential bias in our sampling approach is detailed in Harries et al. (2018). We determine the precision of locating accurate population statistics from a sample of 100 clasts by extrapolating precision estimates from lognormal distributions with similar standard deviations from Rice and Church (1996). They estimate the median of the parent population can be located with an absolute precision of ± 0.84 mm. By performing a two-sample t-test on the log-transformed size distributions of the channel and bar samples at each locality, we identify that the logarithmic mean grain sizes are statistically different between bed structures at a significance level of 0.05, these statistics are included in the supplementary information. We therefore identify that calculating the mean of the composite distribution has the largest source of error in our dataset. To take this into account, we recalculate the composite distributions when the estimates of channel and bar proportions are altered by 10%. The mean values from these distributions define the upper and lower error bars on our measurements. Here we present the arithmetic mean grain size for each site downstream, $\overline{D}_x$, from which we calculate the rate of exponential downstream grain size fining as:

$$\overline{D}_x = \overline{D}_0 e^{-\alpha X} \qquad \textit{Equation 5}$$

where $\overline{D}_0$ is the predicted input mean grain size, X is the downstream distance in km, and α is the fining exponent with units of km^{-1}. We calculate the coefficient of variation (C_v) for each local grain size distribution as

$$C_v = \frac{\sigma}{\overline{D}} \qquad \textit{Equation 6}$$

where σ is the standard deviation measured directly from the local size distribution. Studies suggest that deposits in which there is no spatial trend in C_v downstream are most suitable for the application of the self-similarity model of Fedele and Paola (2007) (e.g. Whittaker *et al.*, 2011; D'Arcy *et al.*, 2017). Harries *et al*. (2018) demonstrate the size distributions on all three fans are broadly self-similar and that there is no statistically significant change in C_v downstream, allowing us to confidently apply the Fedele and Paola (2007) self-similar solutions.

3.2 Subsidence from seismic data

We construct a 3D model of the Iglesia basins stratigraphy in Petrel™ using 2D seismic interpretations of basin fill obtained from Ruskin (2006). Up to six sequence boundaries, younger than 6.57 Ma, were traced across the seismic grid and used to construct isopach maps of basin fill through time. Neither geophysical nor petrographic information from well logs are freely available for the Iglesia basin, therefore, we convert two-way travel times (TWT) to true vertical depth (TVD) using a lithologically-appropriate reconstruction of the depth-velocity profile for the basin fill. At the surface, the Tertiary sandstones and shales exposed have a similar velocity range, 2-2.6 km/s (Ruskin, 2006), therefore we use a mean value of 2.3 km/s as a velocity at the surface and apply a compaction correction at 1 km depth intervals using a compaction profile published in figure 21.8 of North (1985). We attain a depth-averaged velocity of 2.8 km/s over 3 km of fill, in-line with previous inversions by Snyder (1988).

To test the assumption that the spatial distribution of subsidence has not changed significantly through time, we extract 2D cross sections, parallel to the alluvial fans sampled on the surface, and calculate the rate of subsidence of each sequence boundary using the available age constraints on deposition (i.e. depth/age). The oldest sequence boundary (sb) mapped, sb6, is detectable with high continuity and amplitude and is temporally well constrained in outcrop to 6.57 Ma (Ruskin, 2006). This boundary corresponds with the base of seismic sequence 6 in figure 2. The upper boundary of seismic sequence 6, sb7, is constrained to 5.23 Ma. Sequences younger than sb7 are not well dated, though the minimum age of sequence deposition is constrained to >4.3 Ma, based on magneto-stratigraphy (Ruskin, 2006). As four depositional sequences between sb7 and sb11 were deposited within <1Ma, uncertainty on the age of each sequence boundary is relatively low and comparable to the age uncertainty associated with the dated sequence boundaries. We therefore estimate the age of each of the youngest sequence boundaries assuming a constant rate of sediment accumulation and consider the difference between subsidence profiles of all sequence boundaries to be a function of change in the spatial pattern of accommodation space and uncertainty in accumulation rates through time.

As the seismic survey does not extend to the mountain front, we linearly extrapolate the profile of basin subsidence up to the first surface exposure of bedrock. We consider the error on our extrapolation using two linear, end-member scenarios. The first extrapolates to the easternmost bedrock outcrop at the front of the range, while the second extrapolates to the apex of fan deposition.

3.3 Self-similar grain size fining model

Our model formulation for solving the downstream distribution of grain sizes on an alluvial fan incorporates Fedele and Paola's (2007) self-similar solution for downstream fining of gravel. A complete derivation of this approach is described in Fedele and Paola (2007) and a modified field version is presented in Duller *et al.* (2010) (c.f. Whittaker *et al.*, 2011; D'Arcy *et al.*, 2017). Below we outline the points of our modelling procedure; a more detailed derivation is provided in the appendix.

We define the spatial distribution of tectonic subsidence, r , for each system as a 2D profile, extracted directly from the seismically-derived 3D subsidence model of sb 6, as described in section 3.2. For this, and the total downstream system length, we define the spatial distribution of deposition downstream, $R^*(x^*)$ using equation 3. The sediment flux at any downstream distance, $q(x^*)$, is not defined explicitly but is a function of flux required to fill the accommodation space created by tectonic subsidence and the fraction of basin filling, β; it is determined by solving $q_{s0} = \beta\left[(1-\lambda_p)\int_0^{x*} r^*(x^*)\right]$. By including β we account for the basin being open, allowing sediment to bypass the fan system if the accommodation space is overfilled (β > 1). This variable is an important control on the mass balance of the system (c.f. Paola & Martin, 2012). We compare q_s from the model solutions to first order estimates of sediment flux from the primary and tributary source catchments feeding the fans (figure 1), previously published in table 1 of Harries et al. (2018). These estimates were made using a BQART sediment flux model after Syvitski and Milliman (2007) and are ground-truthed against catchment-averaged cosmogenic denudation rate estimates for the region (Bookhagen & Strecker, 2012; Carretier *et al.*, 2015). For further information see the supplementary material and *Harries et al*. (2018).

Assuming the evolution of the river long profiles are diffusional and have an exponential decay in grain size downstream, a solution for gravel fining dependent on the distribution of R^* (as function of x^*) can be obtained using the following transformation:

$$y^*(x^*) = \int_0^{x^*} R^*(x^*)dx^* \qquad \textit{Equation 7}$$

where y^* integrates the distribution of R^* as a function of dimensionless distance downstream. Fedele and Paola (2007) demonstrate that downstream fining profiles are invariant for a specific distribution of $y^*(x^*)$, and thus, they show the mean grain size for gravels at any point downstream, $\overline{D}(x^*)$, can be expressed as an exponential function of y^* so that:

$$\overline{D}(x^*) = \overline{D}_0 + \sigma_0 \frac{C_2}{C_1}(e^{-C_1 y_*} - 1) \qquad \textit{Equation 8}$$

where $\overline{D}_0$ and σ_0 are the mean and standard deviation of the input size distribution at x_0 and C_1 and C_2 are constants that describe how the total grain size variance in the gravel supply is partitioned into local site variation (C_1) and variation down-system, which manifests as a downstream change in $\overline{D}$ (C_2). We define $\overline{D}_0$ as the intercept of an exponential fining curve fit to the observed grain size data and scale σ_0 to $\overline{D}_0$ using the average C_v measured downstream. Fedele and Paola (2007) demonstrate that in a perfectly self-similar system, the partitioning of the variance into C_1 and C_2 does not depend explicitly on x^* and therefore, can be solved analytically using σ and $\overline{D}$ of gravel deposited at local sites downstream.

$$C_v = \frac{\sigma(x^*)}{\overline{D}(x^*)} = \frac{C_1}{C_2} \qquad \textit{Equation 9}$$

The C_v of self-similar deposits is typically found to lie between 0.7 and 1.0, as observed in field studies (e.g. Fedele & Paola, 2007; Whittaker *et al.*, 2010; Michael *et al.*, 2013). Numerical models suggest C_1 has a limited range and lies between 0.55 and 0.9 (Paola & Seal, 1995; Fedele & Paola, 2007). Consequently C_2 can be approximated. Previous studies have used intermediate values of C_1 , i.e. 0.7, (Duller *et al.*, 2010; D'Arcy *et al.*, 2017), although there are few independently-constrained estimates

of its value in the literature. In this study, we measure C_v from our field grain size data, and we use C_1 = 0.7, consistent with D'Arcy *et al.* (2017).

We first present the results from this model and compare the fit to the grain size data collected in the field. The model is then adapted to analyse the impact of lateral inputs of sediment on the grain size fining curves. The diagram in figure 3 depicts the modifications made to the model in order to replicate the processing of lateral sediment inputs in natural settings. The first adapted model, (the tributary model) is modified so that the sediment fill in the basin is not solely supplied by a single apex point source, but is partitioned between several tributary point sources. The distance downstream of each tributary confluence is measured from satellite imagery for the respective fan and is a fixed variable in the model. To avoid the necessity for quantitative constraint on the sediment supply from different inputs, we distribute 100% of the Q_s in each model run between the primary and tributary catchments using their ratios of BQART sediment supply estimates, reported in table A1 and *Harries et al.* (2018). As a first order approximation, this allows us to account for the relative size of each tributary catchment supplying sediment to the system. The second adapted model (the recycling model) mixes a sediment flux with a particular grain size distribution with the trunk-stream supply at each downstream node along the length of the system. This process replicates the continual addition of sediment into the modern system by river incision and surface reworking.

At each lateral input node, a mixing model incorporates an additional sediment flux with a self-similar grain size distribution, into the trunk-stream.

$$\overline{D}_{mixed} = \overline{D}_m \left(\frac{Qs_m}{Qs_m+Qs_t}\right) + \overline{D}_t \left(\frac{Qs_t}{Qs_m+Qs_t}\right) \qquad \text{Equation 10}$$

The mean grain size downstream of the input node, $\overline{D}_{mixed}$, is a function of the mean grain size and sediment flux upstream of the input, $\overline{D}_m$ and Qs_m, and the mean grain size and sediment flux in the tributary, $\overline{D}_t$ and Qs_t. The standard deviation of the mixed sediment supply, σ_{mixed}, is scaled to $\overline{D}_{mixed}$ using C_v. The profile of mass extraction downstream, y^*, is altered so that the spatial

distribution of deposition, R^*, is integrated from the downstream distance of each new lateral input node, x_i^*.

$$y^*(x^*) = \int_{x_i^*}^{x^*} R^*(x^*)dx^* \quad \text{Equation 11}$$

The profile of deposited grain sizes downstream of a lateral input is:

$$\overline{D}(y^*(x^*)) = \overline{D}_{mixed} + \sigma_{mixed}\frac{C_2}{C_1}(e^{-C_1 y_*} - 1) \quad \text{Equation 12}$$

In the special case $\overline{D}_{mixed} \approx \sigma_{mixed}\frac{C_2}{C_1}$ this reduces to a simple exponential

$$\overline{D}(y^*(x^*)) = \sigma_{mixed}\frac{C_2}{C_1}e^{-C_1 y_*} \quad \text{Equation 13}$$

In this paper we introduce another possibility, i.e. that an exponential form can result even when the criterion $\overline{D}_{mixed} \approx \sigma_{mixed}\frac{C_2}{C_1}$ is not met. We refer to this as an 'empirical' exponential, where A is the input grain size and B is fining exponent.

$$\overline{D}(y^*(x^*)) = Ae^{-By_*} \quad \text{Equation 14}$$

We suggest that this form can occur as a consequence of the complexity of the system.

3.4 Model analysis

To analyse the sensitivity of the grain size fining trends observed in the field to changing boundary conditions, we determine the range of model best fit solutions that could statistically describe the measured data, each of which has an associated likelihood. We estimate the best fit of the theoretical models of the form (12) or (14) to the measured data by calculating the log-likelihood function, $\hat{l}$, from the residual sum of squares (RSS) for each hypothesis $H(x) = f(x)$. For each theoretical model, we derive the maximum likelihood estimate, $\hat{f}(x_i)$, attained by varying parameters, k, to fit the model, y, to the measured data, x, with n data points.

$$\hat{l} = -\frac{n}{2}\ln\left[\sum_{i=1}^{n}\left\{\left[(y_i - \hat{f}\ (x_i)\right]^2\right\}\right] = -\frac{n}{2}\ln(RSS) \quad \text{Equation 16}$$

The maximum likelihood solution for the model parameters is determined by fitting the measured data to the different hypotheses using a non-linear least squares regression. We then distinguish between the competing models using the likelihood ratio, calculated from the log-likelihood difference between the theoretical model, $\widehat{l_2}$, and empirical exponential, $\widehat{l_1}$.

$$\widehat{l_2} - \widehat{l_1} = -\frac{n}{2}[\ln(RSS_2) - \ln(RSS_1)] \quad \text{Equation 17}$$

$$\frac{L_2}{L_1} = \exp\{\widehat{l_2} - \widehat{l_1}\} \quad \text{Equation 18}$$

The strength of the evidence for a preference or similarity between models *1* and *2* depends on the likelihood ratio (L_2/L_1) (Kass & Raftery, 1995). Hypothesis *2* is formally indistinguishable from hypothesis *1* if $L_2/L_1 \approx 0$. Hypothesis *2* is preferred over hypothesis *1* when the likelihood ratio, L_2/L_1, is equal to or greater than 1. L_2/L_1 in the range of 1-3 has a preference for hypothesis 2 that is 'slight', 3-10 is 'substantial', 10-30 is 'strong' (Lee & Wagenmakers, 2014).

For the original model of Fedele and Paola (2007), with a single apex input of sediment, we derive a maximum likelihood best fit by systematically varying two broadly constrained variables within the model: the fraction to which the basin is filled, β, between 0.6 and 2.0, and the sediment transport coefficient, C_1, between 0.6 and 0.8. With the tributary model, we systematically vary the mean grain size of all lateral inputs, $\overline{D}_t$, between 2 and 80 mm, and the fill fraction, between 0.6 and 6. These ranges are sensible limits set by the range of gravel grain sizes we observed in the field and by sediment volumes that are plausible for the Iglesia basin based on estimates of catchment sediment fluxes (*Harries et al.,* 2018). The sensitivity of the fit to varying parameters is analysed in contour plots of the ratio of log-likelihood estimates, $f(x)$. We extract the model solutions that fall within 10% of the maximum likelihood best fit and rerun the model with these parameters fixed, varying a third grain size parameter; the mean grain size, $\overline{D}_t$, supplied by tributaries in the upper fan. For the recycling model, we vary three independent variables simultaneously: the mean grain size of the lateral inputs between 2 and 80 mm, the fill fraction, between 0.6 and 6, and the supply rate of recycled sediment,

which in this 2D model is scaled to rates of vertical incision, between 0.1 and 5 m / 10 kyrs. For both lateral input models, we consider a good fit to the data to fall within 10% of the maximum likelihood best fit, which roughly corresponds to solutions that produce a fining rate within one standard deviation of the best fit empirical model.

With this approach we highlight the range of model solutions that could statistically describe the observed grain size data. To quantify how tributary inputs and sediment recycling can buffer the sensitivity of grain size fining trends to changing boundary conditions, we experiment with altering the subsidence rate in the basin. We fix the free variables in the model with the best fit solution for the respective models and vary the subsidence rate in the basin by 0.5, 2 and 4 times the present rate to emulate a range of plausible scenarios for the Iglesia basin (Allmendinger *et al.*, 1990). We also investigate what profile of subsidence would be inverted from the grain size data using the original model when Q_s is constrained by sediment flux estimates from the BQART model and the basin is assumed 100% filled. The subsidence profile is given an exponential form with a wavelength set by the width of the basin and we experiment with changing the exponent of the solution. The results from these two experiments are presented in summary figures 9 and 10 and are discussed in section 5.1.

4. Results

4.1 Basin subsidence

From the late Miocene to present, the locus of the maximum rate of subsidence in the Iglesia basin has been approximately 20-30 km from the mountain front. In figure 4, our 3D basin model indicates that the profile of subsidence varies considerably along strike of the front. For all six sequence boundaries (sb) analysed, isopachs highlight two subsidence centres, north and south of the basin axis (Appendix figure A3). Maximum subsidence is focused south of the basin axis, where sb6 (6.57 Ma) and sb7 (> 4.3 Ma) reach depths of 2000 m and 1400 m (figure 4), respectively. From this depo-centre, subsidence decreases rapidly toward the southern basin margin, where seismic sequences onlap

457 Palaeozoic basement. North of the basin axis, the pattern of subsidence is broader, where sb6 plateaus
458 around depths of 1500-1700 m and sb10, around 800-900 m. The northern margin of the basin is not
459 imaged. Uplift on the south eastern margin of the basin correlates in space to the footwall of a positive
460 flower structure, associated with the northern termination of the El Tigre strike slip fault system
461 (figure 2).

462 The pattern and rate of subsidence through time in transects parallel to our measurement sites is
463 examined in 2D cross sections in figure 5. There is a broad agreement between the amplitude and
464 shape of the subsidence profiles derived for dated sb 6 and 7 for each respective fan. Fan 2 has the
465 highest rate of subsidence 2.25 ± 0.1 m/ 10 kyr at its toe, ~25 km downstream from the fan apex. Fan
466 3 has a shallower subsidence profile that plateaus ~ 18 km downstream from the fan apex to the fan
467 toe with a maximum rate of subsidence of 1.55 ± 0.05 m/ 10kyr. The maximum rate of subsidence on
468 fan 1 is 1.8 ± 0.1 m/10 kyr and is located ~30 km from the fan apex. As fan 1 is longer than the other
469 two fans, we observe subsidence decreasing downstream toward the toe to 1.2 m/10 kyr. The younger
470 sequence boundaries, 8-11 also have a similar wavelength of subsidence and if we assume constant
471 sedimentation rate through time, we find the maximum difference in the rate of subsidence between
472 all sequence boundaries is relatively small; 0.2-0.5 m/10 kyr for all fans. In the absence of any evidence
473 suggesting a marked change in subsidence through time, we conclude that the rate and pattern of
474 subsidence has remained the same since the Late Miocene and we apply the subsidence profile of sb
475 6 as a boundary condition for Quaternary deposition in our model.

476 The amount of accommodation space produced by subsidence, calculated from a 2D area integration
477 of the subsidence profile for sb 6, is estimated ~8500, ~9300 and 7600 m^2/ 10 kyr for fan 2, fan 1 and
478 fan 3, respectively. This is the space made available for mass extraction within the self-similar fining
479 model. Assuming 30 % porosity for gravel in the basin fill (Allen & Allen, 2013), the average
480 accumulation rates required to fill the accommodation space are ~0.65, 0.60 and 0.53 m/ 10 kyr, for
481 fans 1, 2 and 3, respectively. These estimates are in line with accumulation rates derived by Ruskin

(2006) from magnetostratigraphy of basin fill outcrops exposed in the east of the basin, which suggest average millennial accumulation rates of <1 m/ 10 kyrs for the early Pliocene.

4.2 Modelling grain size fining

4.2.1. Empirical model

The mean grain size of river bed sediment measured at site 1, taken to be the input mean grain size at X_0, is 93 mm on fan 1, 164 mm on fan 2 and 119 mm on fan 3 (table 1). Downstream, the mean grain size fines exponentially with exponents of 1.8 % / km on fan 1, 6.7 % / km on fan 2 and 5.9 % / km on fan 3. These fining rates are an order of magnitude greater than would be expected from abrasion alone for our resistant lithologies (Attal *et al.*, 2006; Attal & Lavé, 2009), supporting our assumption that abrasion is not the main control on sediment fining across the studied fans. These fining rates are the same order of magnitude as those measured in Eocene Pablo basin, Spanish Pyrenees (Whittaker *et al.*, 2011) and Holocene fans in Death Valley (D'Arcy *et al.*, 2017). They are an order of magnitude greater than would be expected from abrasion alone for extrusive and intrusive gravel, typically less than 0.3 % / km (Attal *et al.*, 2006; Attal & Lavé, 2009). However, because our gravel contains a significant proportion of sedimentary rocks, we have to assess whether the preferential abrasion of sedimentary rocks could lead to such downstream fining. The analysis presented in Appendix A2 shows that the influence of abrasion is likely minimal on fans 2 and 3, therefore supporting our initial assumption, but that abrasion may contribute to a maximum of 30 % of the downstream fining on fan 1. For simplicity, we focus in the following on the potential influence of tributary input and recycling on grain size trends, and present results that do not account for abrasion. We highlight that the influence of abrasion should be considered in cases where the sediment transported on fans is highly erodible. In the case of fan 1, we note that not taking into account the effect of abrasion may lead to an overestimating of the volumes of sediment required to fit the data, but the overall patterns and interpretations are not affected.

On figure 6, we highlight 95% (2σ) and 68% (σ) confidence bounds for the non-linear least squares regression of the exponential to the measured data. Scatter in mean grain size of fan 1's upper reach reduces the confidence of the exponential fit to the data; this is reflected in a relatively high RMSE of 12.07 and a $\widehat{l_1}$ of 7.29. An exponential model fit to fan 2's data has a RMSE of 23.02, a $\widehat{l_1}$ of 8.35 and wide confidence intervals. Fan 3's regression has a RMSE of 7.17, a $\widehat{l_1}$ of 6.02, and narrow confidence bands, reflecting the limited scatter in the dataset and the excellent fit of an exponential function.

4.2.2. Single source model

The 2D model solution for a system with a single apex input of sediment predicts (after Fedele & Paola, 2007) for all fans, that the mean grain size fines slowly from the fan apex across the upper reach of the fan, and then fines rapidly in the lower reaches, producing a convex fining profile (red lines, figure 6). This trend is fundamentally driven by the fact that accommodation space is limited in the upper reaches of the fans and increases markedly down fan toward the basin centre (figure 5), leading to increasing rates of sediment extraction and increased fining down-fan. Under no sediment supply or bedload mobility scenario can the single apex model reproduce the exponential pattern of grain size fining observed in the field, as demonstrated in figure 6.

4.2.3. Tributary model

Tributary catchments are estimated to supply 46% of the total sediment flux to fan 1 (table A1). We find that for the first iteration of the model, a mean tributary input grain size of 60 mm and a basin that is over supplied with sediment (β = 2) produces a likelihood ratio of 0.35 and is therefore indistinguishable from the empirical model (figure 7a). The maximum likelihood ratio of 5.5 is achieved when the grain size of the upper fan tributaries is allowed to vary independent of the down fan tributaries, showing that the tributary model fits better than the empirical exponential model. This best fit solution has a fine, ~20 mm, tributary input in the upper fan and a coarse, 60 mm, input in the lower fan (figure 7a (ii)). However, solutions that have a likelihood ratio > 1 also show a preference for the tributary model over the empirical model (eq. 14) and fall within 1σ error of the latter model.

These solutions, plotted in plot 7a (i), can be generated for a moderate range of basin fill fractions, 2.0-6.0, and tributary grain sizes <50 mm. By distributing the two sediment input points downstream, the tributary model can, therefore, produce a grain size fining profile that is statistically similar to that observed in the field for a number of basin fill and input grain size scenarios. Although we do not have detailed grain size data for these lateral inputs, the values predicted are consistent with the types of grain size supplied by catchments in this area (Harries *et al*., 2018).

Tributaries supply 68% of the total catchment flux to fan 3, in two main locations. Contour plot c (ii) in figure 7 shows a maximum likelihood ratio of 0.4 is attained for the best fit solution where the basin is slightly over-filled (β = 1.2) and the lateral input mean grain size is ~ 40 mm (first iteration). The likelihood ratio is not improved by varying the grain size of different tributaries independently (second iteration). The tributary model is indistinguishable from the empirical model in this case. Solutions with likelihood ratios > 0 also fall within 2σ of the empirical model and are plotted as downstream fining curves in figure 7c (i). These solutions cover a range of basin fill fractions, 0.8-1.5, and grain sizes, <70 mm.

Fan 2's grain size fining profile cannot be effectively reproduced using the tributary model. As shown in plot 7b, the best fit solution deviates little from the single apex model solution. There is a clear preference for the empirical model with a likelihood ratio of 10^{-4}. This is due to the fact that the main tributary input occurs at > 10 km downstream and contributes only 18 % of the total catchment supply, a flux that is evidently too small to have a significant impact on the grain size fining profile, irrespective of the grain size of the lateral input.

4.2.4. Recycling model

The recycling model applied to fan 1 achieves a maximum likelihood ratio of 0.9, indicating the recycling model is indistinguishable from the empirical exponential (figure 8a (ii)). As with the tributary model, the best fit to the measured data is attained with a coarse mean lateral input grain size of 60 mm (figure 8a (ii)). The rate of incision that best fits the data is between 3 and 4 m / 10 kyr. However,

556 in plot 8a (i) we show model solutions that have a likelihood ratio > 0.1 also fall within a 1σ error of
557 the empirical model, which encompasses a wide range of possible rates of incision, 0.1 – 5 m / 10 kyr,
558 and the full range of grain sizes tested. We do not have extensive grain size measurements of the fan
559 surfaces being incised, however the range of grain sizes predicted by the model were observed both
560 on the terrace surfaces and in cross-section.

561 A statistical fit to fan 3's grain size fining profile is also indistinguishable from the empirical model with
562 a maximum likelihood ratio of 0.6 (figure 8c (ii)). A best fit to the data is attained with 1 m / 10 kyr of
563 incision and the recycling of gravel with a mean grain size of 2 mm in a basin that is 100% filled (β=1).
564 Solutions with a likelihood ratio > 0.05 fall within 1σ error of the empirical model, plotted in figure 8c
565 (i), and are well constrained to a narrow range of grain sizes, <30 mm, and incision rates, 0.1-2.5 m /
566 10 kyr.

567 For fan 2, the recycling model produces a fit with a maximum likelihood ratio of 1.4 and is therefore
568 slightly preferred over the empirical model (figure 8b (ii)). As with fan 3, the best fit solution has a
569 mean lateral input grain size of 2 mm and 1 m / 10 kyr of channel incision. However, solutions with a
570 likelihood ratio of > 0.2 fall within 1σ error of the empirical model, plotted on figure 8b (i), and are
571 attained for the full range of recycled fluxes and basin fill fractions tested.

572 ## 5. Discussion

573 With unique constraints on the subsidence profile of the Iglesia basin and therefore the time-
574 integrated distribution of mass extraction downstream, we have demonstrated that a classical 2D
575 single source self-similarity grain size fining model (Fedele & Paola, 2007) cannot reproduce observed
576 rates of downstream sediment fining in the modern rivers that deliver material to the alluvial fans
577 filling the Iglesia basin. We show that from fan apex to toe, the mean grain size of gravel deposited on
578 the river bed of each fan decreases exponentially. This reduction in grain size primarily occurs in the
579 upper reaches of each fan, despite there being little accommodation space to drive a reduction in
580 sediment calibre by size-selective mass extraction. However, by developing our grain size model to

include lateral inputs of sediment, we show additional sediment supplied downstream of the apex source can markedly modify the spatial distribution of mass supplied to the sediment routing system and alter the profile of downstream grain size fining.

Lateral inputs of sediment have been considered a source of noise in downstream grain size trends (Knighton, 1980; Hoey & Bluck, 1999; Gomez *et al.*, 2001) and there is certainly evidence of this on the Iglesia basin fans where tributary confluences correlate in space with substantial fluctuations in mean grain size. While we aimed to limit the impact of local slope and grain size variability at tributary confluences by sampling at distance from the input, autogenic adjustments of the bed surface slope to local fluctuations in water discharge, sediment flux and grain size may impact local grain size variability. Furthermore, a lack of synchronicity between sediment transport events in the main stream and channel may bias sampling toward more recent events. This transient variability introduces scatter in the downstream grain size fining profiles and reduces the sensitivity of the model fit to the data. For example, a greater scatter in the dataset of fan 1 compared to fan 3 means a larger combination of free parameters can be used to fit to the measured data, thereby reducing the effective sensitivity of the modelling. Importantly, however, we demonstrate when we consider transient, local variability in grain size as only a source of scatter in the grain size profiles of depositional systems, we find lateral inputs, defined by their flux and grain size alone, have a significant influence on the long term mass balance of the depositional system and their downstream grain size fining trends. Lateral sediment inputs can therefore be a driver of downstream fining.

With the tributary model, we find the profile of grain size fining can be modified by lateral inputs but only if the sediment flux from the input is relatively large and the grain size of the input is dissimilar to that of the trunk stream. For example, on fan 2, only 18 % of the total catchment flux is supplied by tributaries with little impact on the grain size fining trend, irrespective of input calibre. In contrast, tributaries supply fans 1 and 3 with 46 % and 68 % of their total catchment supply, respectively, which is a large enough to modify the grain size fining profile. As point sources, tributaries can create steps

606 in the grain size fining profile that emulate changes in the measured profile downstream of
607 confluences (Rice 1998; 1999). A good statistical fit to the measured fining trends on these fans can
608 be achieved with the addition of medium sized gravel in the upper fan. This finer input is necessary in
609 order to induce fining on a reach with minimal subsidence. The best fit solution for fan 1 additionally
610 requires tributaries further downstream to introduce large fluxes of coarse gravel, in order to maintain
611 the very low rates of grain size fining observed. These sediment flux scenarios are in broad agreement
612 with the first order estimates of sediment fluxes made by Harries et al. (2018) using a BQART model
613 (table A1). The source catchments of fans 3 are estimated to supply ~12,000 m^2 / 10 kyr of sediment,
614 which is comparable to the flux of sediment predicted by the fining model, 16,000 ± 5500 m^2 / 10 kyr.
615 For fan 1, the fining model predicts sediment fluxes >38,000 m^2 / 10 kyr provide a good fit to the grain
616 size data, which is larger than that estimated by the BQART model, ~25,000 m^2 / 10 kyr. Here it should
617 be recognised that although these BQART estimates are in line with cosmogenic erosion rates derived
618 for the region, they are subject to major uncertainties with regards to the proportion of the flux that
619 is transported as bedload (Harries *et al.*, 2018).

620 Unlike the tributary model, the recycling model reproduces a smooth exponential fit to the data as
621 sediment is supplied continuously downstream. The recycling of old fan surfaces is evident in the field
622 (figure 1) and our modelling suggests these lateral inputs alone could account for deviations in the
623 grain size fining profiles for all three fans. The best fit model solutions for fans 1 and 3, however, are
624 similar to the tributary model solutions; fan 1 requires a large input of coarse sediment to maintain its
625 low rate of grain size fining, whereas the smaller fans 2 and 3 require a small input of fine gravel to
626 initiate fining in the upper fan. A flux of predominantly fine gravels onto the bed surface could arise if
627 the recycled surface is enriched in finer gravels relative to the Holocene catchment supply, or equally,
628 if the surfaces are similar in size composition but the Holocene discharge regime is less competent in
629 transporting the same coarse size distribution. With no constraint on the flux of recycled material
630 supplied to the model, we find the best fit solutions for fans 2 and 3 involve a rate of vertical incision
631 into older fan surfaces of ~1 m / 10 kyr, which approximates the average channel depth in a Holocene

surface measured in the field (figure 1). This ground-truthing of the model results gives strength to our model outcomes being reasonable. The recycling solution for fan 1 indicates a rate of vertical incision of 4-5 m / 10 kyr is required to sustain the low rate of downstream grain size fining observed. Unlike fans 2 and 3, fan 1 is currently incising into a series of older generation surfaces; lack of good age constraints on these surfaces does not allow us to support or reject this model solution. It is likely, however, that both tributaries and the recycling of sediment, contribute to the exponential downstream fining trends on fans 1 and 3 and that one end member solution does not fully capture the sediment dynamics of the system (eq.13).

As well as being sensitive to the flux and calibre of lateral inputs, the fining profile is also controlled by the filled state of the basin or, alternatively, the percentage flux that bypasses the basin. The gravel-sand transition is typically correlated with downstream distance at which the bedload supply of gravel is exhausted, and is a good indicator of basin fill. For both lateral input models, best fit solutions for the smaller fans 2 and 3 indicate the basin is approximately filled. These solutions are in agreement with the fact that we observed a clear gravel-sand transition on both of the fans, which we use as a marker for the maximum downstream distance of the fan. We do not observe a gravel-sand transition on the largest fan 1 and, instead, mark the maximum downstream distance as the confluence of its main channel with the axial drainage system. With no apparent exhaustion of the gravel supply before this distance, there is evidence to suggest large fluxes of gravel are bypassing the fan. This is supported by the absence of any significant tributary mouth accumulations that would otherwise indicate sediment storage upstream. In line with these observations, our best fit model solutions for fan 1 suggest this system has a catchment supply that is at least twice of what can be stored in the basin, implying that at least 50% of its catchment supply of gravel is bypassing the basin.

5.1 Sensitivity to external boundary conditions

Using 2D self-similar models, we demonstrate lateral inputs of sediment in large alluvial systems are an important driver of downstream grain size fining as demonstrated in the Iglesia basin where we

657 can observe grain size fining in the upper reaches of three alluvial fans despite little available
658 accommodation space to drive selective mass extraction. From our data, we find the downstream
659 fining trends on each of the Iglesia basin fans can be explained if they are considered an integrated
660 signal of both the catchment and fan responding to Holocene environmental change. This implies an
661 external boundary condition change could be masked by dynamic depositional responses to forcing.
662 Using the recycling model we explore whether grain size fining trends might still be sensitive to
663 subsidence forcing in spite of signal masking. Here we assume that a change in subsidence rate is not
664 accompanied by a change in the rate or character of sediment recycled and there is no alteration in
665 how the drainage network of channels is configured. In summary figure 9a-c, a halving of the
666 subsidence rate does not produce a fining curve that is statistically dissimilar from the modern
667 subsidence rate. As our modelling predicts that the basins are at least filled and likely overfilled at
668 present, a decrease in accommodation space for the same sediment supply would result in a greater
669 rate of sediment bypass and a fining curve relatively insensitive to any excess of sediment. This loss of
670 sensitivity to greater basin fill fractions was originally highlighted in Duller *et al.* (2010) and is clearly a
671 major control on fining in the Iglesia basin. A quadrupling of the subsidence rate does provide a profile
672 of grain size fining that is statistically different from the modern profile. Fining occurs more rapidly
673 and, on all fans, the gravel supply is exhausted upstream of the modern fan toe. The effect is most
674 pronounced on fan 1 where an under-filling of the basin has resulted in a gravel runout distance that
675 is ~40% shorter than the modern system, equivalent to ~15 km of gravel retreat. On fans 2 and 3, the
676 gravel runout distance is ~20% shorter than the modern system, equivalent to ~5 km of gravel retreat.
677 This suggests that downstream grain size fining profiles, although buffered, can still be sensitive to
678 changes in their boundary conditions that are of sufficient magnitude and in the right direction (i.e.
679 towards greater subsidence).

680 ### *5.2 Wider implications and future work*
681

682 This work highlights the importance of both the tectonic boundary conditions and the locus of
683 sediment inputs on the spatial distribution of mass extraction in a basin. It is therefore important to
684 ask whether sediment recycling and tributaries are a source of "noise" in downstream grain size fining
685 trends, or whether they are an important part of the signal. We argue that inversions of downstream
686 fining profiles require us to consider the entire sediment routing system and its response to forcing,
687 and not just the trunk stream. This approach better captures how the complex response of Quaternary
688 alluvial fans to climatic change, where fan surface generation, abandonment and incision is typically
689 observed, manifests in the geological record (Malatesta *et al.*, 2018).

690 This line of thinking also raises an important question: what should be considered the source of
691 sediment in source-to-sink sediment routing models? Single apex models are not capable of describing
692 the complexity of sediment sourcing dynamics in these large alluvial systems. The volumes of
693 sediment recycled from Holocene fan surfaces can be comparable if not greater than the volumes
694 supplied by catchments alone (*D'Arcy et al., 2017*; Harries *et al., 2018*), demonstrating that alluvial
695 piedmonts are themselves important sources of sediment at least over intermediate timescales (10^2-
696 10^3 years). Beyond the implications for quantitative reconstructions of basin stratigraphy, this sourcing
697 problem also has an important inference for provenance studies using river bed gravels to reconstruct
698 source region dynamics and for the application of cosmogenic nuclides in dating surface exposures
699 and calculating catchment average erosion rates (Nichols *et al.*, 2005; von Blanckenburg, 2006;
700 Wittmann *et al.*, 2011; Covault *et al.*, 2013; Foster *et al.*, 2017; Mason & Romans, 2018). These
701 approaches typically rely on an assumption that the population of gravel in a stratigraphic horizon or
702 bed surface is deposited instantaneously on a geological time frame, whereas we find the river bed
703 surface is likely a recycled mixture of sediment cascading through the depositional realm over time.

704 In terms of reconstructing environmental boundary conditions from deposited grain sizes, the extent
705 to which the spatial distribution of tectonic subsidence or the sediment budget of the system may be
706 over or under-estimated by a lack of constraint on lateral sediment supplies needs to be considered

(c.f. Allen, 2008; Duller *et al.*, 2010; Armitage *et al.*, 2011; Allen *et al.*, 2013). The magnitude of sediment recycling and the geographical stability of tributary inputs over geological time-frames are variables that are important to constrain, though they are often unknowable for the geological past. Without this constraint, we have demonstrated inversions of basin structure and evolution could deviate significantly from reality. The two lateral input end member models newly developed in this study simplify the geomorphology of each system to include lateral inputs that are spatially uniform or point source specific. These models fall short of capturing the full spatial complexity of lateral sediment addition, however, they highlight the importance of considering lateral sediment input in models of sediment routing. Ground-truthing of the model results, with measurements of the grain size supplied by tributaries and recycled material, would corroborate whether the end member models do a good job at simplifying the geomorphology of the system.

6. Conclusions

With unique constraint on the external boundary conditions for sediment deposition in the Iglesia basin, we show how lateral sediment inputs exert a first order control on the profile of grain size fining in alluvial fan systems. For the three alluvial fans studied here, seismic mapping of dated sequence boundaries reveals subsidence increases away from the mountain front and along strike of the mountain front, with maximum rates of subsidence of 2.25 m / 10 kyr in the south and 1.55 m / 10 kyr in the north. Using a self-similar downstream grain size fining model constrained with measured subsidence profiles, we find we cannot reconstruct the profile of downstream grain size fining measured on the active river bed of each fan for any sediment supply scenario using a point source at the apex of the fans. This is because we observe fining in the upper fan where the model predicts downstream fining ought to be minimal due to the limited amount of accommodation space required to induce deposition. However, we develop the self-similarity model to incorporate bedload mixing and we demonstrate lateral inputs of sediment are key for replicating the Holocene grain size profiles on all fans.

We simplify the spatial variability in lateral inputs to two end-member models, a tributary model, adapted with two free parameters in the fraction of basin fill and the mean grain size of the lateral input, and a sediment recycling model, adapted with three free parameters in the fraction of basin fill, the recycled flux and the mean grain size of recycled material. For fans 1 and 3, the tributary model can produce profiles of grain size fining that provide a better fit or a fit indistinguishable from an empirical exponential model. These two fans have tributary fluxes that make up > 46 % of the total catchment sediment supply, which contrasts with fan 2, whose tributaries supply ~ 18 % of the total catchment flux. Here, the tributary model does not provide a better fit than the single input model for fan 2 as its tributary contributions are too small. The best fit solution for fan 1 requires coarse gravel, $\overline{D}$ ~ 60 mm, to be supplied by the lower tributaries and fine gravel, $\overline{D}$ ~ 20 mm, to be supplied by the upper tributaries, and for the basin to be over filled ($\beta \geq 2$). Data from fan 3 are best fit with an addition of medium gravel, $\overline{D}$ ~ 40 mm, and a basin slightly over filled ($\beta = 1.2$). The recycling model provides a better fit or a fit indistinguishable from an empirical exponential model for all three fans. Both fans 2 and 3 are best fitted with a moderate flux of recycled fine gravel ($\overline{D}$ ~ 2 mm), equivalent to incision rates of 1 m / 10 kyr, consistent with field observations. The best fit solution for fan1 requires a large flux of coarse gravel ($\overline{D}$ ~ 60 mm), equivalent to incision rates of 3-4 m / 10 kyr. The range of lateral input model solutions that can fit the data to within 1σ of the exponential rate of downstream fining increases as scatter in the data increases. The sensitivity of the fit to varying the free parameters in the lateral input models is, therefore, relatively low for fan 1 (RMSE = 12.07), but high for fan 3 (RMSE = 7.17).

This relatively simple approach to incorporating complex sediment sourcing dynamics into grain size fining models has significant implications for how we interpret climatic and tectonic forcing from stratigraphic grain size trends. Fining trends are a predictable function of basin accommodation and sediment flux, but this sensitivity is masked by the complexity of sediment sourcing dynamics within the depositional basin. Quantitative inversions of large alluvial systems therefore need to consider lateral inputs of sediment as a major control on grain size fining, as grain size fining model solutions

759 which assume a single sediment source input may wrongly predict sediment fluxes or tectonic
760 subsidence distributions in circumstances where lateral inputs drive down-system grain size profiles.

761 Acknowledgments
762

763 We thank Trevor Hoey and Julieta Suriano for their insightful reviews that helped improve the
764 manuscript. This work was funded by NERC E^3 DTP Studentship NE/L002588/1 and The School of Geosciences
765 at The University of Edinburgh.

766 References
767

768 ALLEN, P.A. & DENSMORE, A.L. (2000) Sediment Flux from an Uplifting Fault Block. *Basin Research*, **12,**
769 367-380.
770 ALLEN, P.A. (2008) From Landscapes into Geological History. *Nature*, **451,** 274-276.
771 ALLEN, P.A. & HELLER, P.L. (2012) Dispersal and Preservation of Tectonically Generated Alluvial Gravels
772 in Sedimentary Basins. *Tectonics of Sedimentary Basins: Recent Advances***,** 111-130.
773 ALLEN, P.A. & ALLEN, J.R. (2013) *Basin Analysis: Principles and Application to Petroleum Play Assessment*,
774 3rd edition edn. Wiley.
775 ALLEN, P.A., ARMITAGE, J.J., CARTER, A., DULLER, R.A., MICHAEL, N.A., SINCLAIR, H.D., WHITCHURCH, A.L. &
776 WHITTAKER, A.C. (2013) The Qs Problem: Sediment Volumetric Balance of Proximal Foreland
777 Basin Systems. *Sedimentology*, **60,** 102-130.
778 ALLEN, P.A., MICHAEL, N.A., D'ARCY, M., RODA-BOLUDA, D.C., WHITTAKER, A.C., DULLER, R.A. & ARMITAGE, J.J.
779 (2017) Fractionation of Grain Size in Terrestrial Sediment Routing Systems. *Basin Research*,
780 **29,** 180-202.
781 ALLMENDINGER, R.W., FIGUEROA, D., SNYDER, D., BEER, J., MPODOZIS, C. & ISACKS, B.L. (1990) Foreland
782 Shortening and Crustal Balancing in the Andes at 30-Degrees-S Latitude. *Tectonics*, **9,** 789-809.
783 ALVAREZ-MARRON, J., RODRIGUEZ-FERNANDEZ, R., HEREDIA, N., BUSQUETS, P., COLOMBO, F. & BROWN, D. (2006)
784 Neogene Structures Overprinting Palaeozoic Thrust Systems in the Andean Precordillera at 30
785 Degrees S Latitude. *Journal of the Geological Society*, **163,** 949-964.
786 AMANTE, C. & EAKINS, B.W. (2009) Etopo1 1 Arc-Minute Global Relief Model: Procedures, Data Sources
787 and Analysis. N. T. M. N. NGDC-24. National Geophysical Data Center, NOAA.
788 ARMITAGE, J.J., DULLER, R.A., WHITTAKER, A.C. & ALLEN, P.A. (2011) Transformation of Tectonic and
789 Climatic Signals from Source to Sedimentary Archive. *Nature Geoscience*, **4,** 231-235.
790 ATTAL, M. & LAVÉ, J. (2006) Changes of Bedload Characteristics Along the Marsyandi River (Central
791 Nepal): Implications for Understanding Hillslope Sediment Supply, Sediment Load Evolution
792 Along Fluvial Networks, and Denudation in Active Orogenic Belts. *Tectonics, Climate, and*
793 *Landscape Evolution*, **398,** 143-171.
794 ATTAL, M., LAVE, J. & MASSON, J.P. (2006) New Facility to Study River Abrasion Processes. *Journal of*
795 *Hydraulic Engineering-Asce*, **132,** 624-628.
796 ATTAL, M. & LAVÉ, J. (2009) Pebble Abrasion During Fluvial Transport: Experimental Results and
797 Implications for the Evolution of the Sediment Load Along Rivers. *Journal of Geophysical*
798 *Research-Earth Surface*, **114**.
799 ATTAL, M., MUDD, S.M., HURST, M.D., WEINMAN, B., YOO, K. & NAYLOR, M. (2015) Impact of Change in
800 Erosion Rate and Landscape Steepness on Hillslope and Fluvial Sediments Grain Size in the
801 Feather River Basin (Sierra Nevada, California). *Earth Surface Dynamics*, **3,** 201-222.

BEER, J.A., ALLMENDINGER, R.W., FIGUEROA, D.E. & JORDAN, T.E. (1990) Seismic Stratigraphy of a Neogene Piggyback Basin, Argentina. *Aapg Bulletin-American Association of Petroleum Geologists*, **74,** 1183-1202.

BOOKHAGEN, B. & STRECKER, M.R. (2012) Spatiotemporal Trends in Erosion Rates across a Pronounced Rainfall Gradient: Examples from the Southern Central Andes. *Earth and Planetary Science Letters*, **327,** 97-110.

BUFFINGTON, J.M. & MONTGOMERY, D.R. (1997) A Systematic Analysis of Eight Decades of Incipient Motion Studies, with Special Reference to Gravel-Bedded Rivers. *Water Resources Research*, **33,** 1993-2029.

BUNTE, K. & ABT, S.R. (2001) Sampling Surface and Subsurface Particle-Size Distributions in Wadable Gravel-and Cobble-Bed Streams for Analysis in Sediment Transport, Hydraulics and Stream Bed Monitoring, Gen. Tech Rep. Rms-Gtr-74, United States Department of Agriculture, Forest Service, Rocky Mountain Research Station, Fort Collins, CO**,** 428.

CARRETIER, S., TOLORZA, V., RODRIGUEZ, M.P., PEPIN, E., AGUILAR, G., REGARD, V., MARTINOD, J., RIQUELME, R., BONNET, S., BRICHAU, S., HERAIL, G., PINTO, L., FARIAS, M., CHARRIER, R. & GUYOT, J.L. (2015) Erosion in the Chilean Andes between 27 Degrees S and 39 Degrees S: Tectonic, Climatic and Geomorphic Control. *Geodynamic Processes in the Andes of Central Chile and Argentina*, **399,** 401-418.

CHURCH, M. & KELLERHALS, R. (1978) Statistics of Grain-Size Variation Along a Gravel River. *Canadian Journal of Earth Sciences*, **15,** 1151-1160.

CONSTANTINE, C.R., MOUNT, M.F. & FLORSHEIM, J.L. (2003) The Effects of Longitudinal Differences in Gravel Mobility on the Downstream Fining Pattern in the Cosumnes River, California. *Journal of Geology*, **111,** 233-241.

COVAULT, J.A., CRADDOCK, W.H., ROMANS, B.W., FILDANI, A. & GOSAI, M. (2013) Spatial and Temporal Variations in Landscape Evolution: Historic and Longer-Term Sediment Flux through Global Catchments. *Journal of Geology*, **121,** 35-56.

D'ARCY, M., WHITTAKER, A.C. & RODA-BOLUDA, D.C. (2017) Measuring Alluvial Fan Sensitivity to Past Climate Changes Using a Self-Similarity Approach to Grain-Size Fining, Death Valley, California. *Sedimentology* **64,** 388-424 doi:10.1111/sed.12308

DINGLE, E.H., SINCLAIR, H.D., ATTAL, M., MILODOWSKI, D.T. & SINGH, V. (2016) Subsidence Control on River Morphology and Grain Size in the Ganga Plain. *American Journal of Science*, **316,** 778-812.

DULLER, R.A., WHITTAKER, A.C., FEDELE, J.J., WHITCHURCH, A.L., SPRINGETT, J., SMITHELLS, R., FORDYCE, S. & ALLEN, P.A. (2010) From Grain Size to Tectonics. *Journal of Geophysical Research-Earth Surface*, **115**.

FEDELE, J.J. & PAOLA, C. (2007) Similarity Solutions for Fluvial Sediment Fining by Selective Deposition. *Journal of Geophysical Research-Earth Surface*, **112**.

FERGUSON, R.I., CUDDEN, J.R., HOEY, T.B. & RICE, S.P. (2006) River System Discontinuities Due to Lateral Inputs Generic Styles and Controls. *Earth Surface Processes and Landforms* **31,** 1149-1166 doi:10.1002/esp.1309

FERNÁNDEZ-SEVESO, F. (1993) Sismoestratigrafia De La Cuenca Iglesia: Informe De Actividades En La Universidad De Cornell. **Informe Interne 10.408,** 20.

FORZONI, A., STORMS, J.E.A., WHITTAKER, A.C. & DE JAGER, G. (2014) Delayed Delivery from the Sediment Factory: Modeling the Impact of Catchment Response Time to Tectonics on Sediment Flux and Fluvio-Deltaic Stratigraphy. *Earth Surface Processes and Landforms*, **39,** 689-704.

FOSTER, M.A., ANDERSON, R.S., GRAY, H.J. & MAHAN, S.A. (2017) Dating of River Terraces Along Lefthand Creek, Western High Plains, Colorado, Reveals Punctuated Incision. *Geomorphology*, **295,** 176-190.

GOMEZ, B., ROSSER, B.J., PEACOCK, D.H., HICKS, D.M. & PALMER, J.A. (2001) Downstream Fining in a Rapidly Aggrading Gravel Bed River. *Water Resources Research*, **37,** 1813-1823.

HARRIES, R.M., KIRSTEIN, L., WHITTAKER, A., ATTAL, M., PERALTA, S. & BROOKE, S. (2018) Evidence for Self-Similar Bedload Transport on Andean Alluvial Fans, Iglesia Basin, South Central Argentina *Journal Of Geophysical Research: Earth Surface*, **123,** 2292-2315.

HELLER, P.L. & PAOLA, C. (1992) The Large-Scale Dynamics of Grain-Size Variation in Alluvial Basins, 2 Application to Syntectonic Conglomerate, Basin Research Volume 4, Issue 2. *Basin Research* **4,** 91-102

HIRANO, M. (1971) River Bed Degradation with Armouring. *Proceedings of the Japanese Society of Civil Engineering*, **195,** 55-65.

HOEY, T.B. & FERGUSON, R.I. (1997) Controls of Strength and Rate of Downstream Fining above a River Base Level Water Resources Research Volume 33, Issue 11. *Water Resources Research* **33,** 2601-2608

HOEY, T.B. & BLUCK, B.J. (1999) Identifying the Controls over Downstream Fining of River Gravels. *Journal of Sedimentary Research*, **69,** 40-50.

HOVIUS, N. & LEEDER, M. (1998) Clastic Sediment Supply to Basins. *Basin Research*, **10,** 1-5.

HUMPHREY, N.F. & HELLER, P.L. (1995) Natural Oscillations in Coupled Geomorphic Systems - an Alternative Origin for Cyclic Sedimentation. *Geology*, **23,** 499-502.

JEROLMACK, D.J. & PAOLA, C. (2010) Shredding of Environmental Signals by Sediment Transport. *Geophysical Research Letters*, **37**.

JORDAN, T., FERNANDEZ, A., FERNANDEZ-SEVESO, F., RÉ, G. & MILANA, J.P. (1997) Relaciones Entre Las Historias Evolutivas De Las Cuencas De Iglesia Y Bermejo, Prov. De San Juan, Argentina. *Actas de las segundas jornadas sobre geologia de Precordillera***,** 142-147.

KASS, R.E. & RAFTERY, A.E. (1995) Bayes Factors. *Journal of the American Statistical Association*, **90,** 773-795.

KELLERHALS, R. & BRAY, D.I. (1971) Improved Method for Size Distribution of Stream Bed Gravel. *Water Resources Research*, **7,** 1045.

KNIGHTON, A.D. (1980) Longitudinal Changes in Size and Sorting of Stream-Bed Material in 4 English Rivers. *Geological Society of America Bulletin*, **91,** 55-62.

LAMB, M.P., DIETRICH, W.E. & VENDITTI, J.G. (2008) Is the Critical Shields Stress for Incipient Sediment Motion Dependent on Channel-Bed Slope? *Journal of Geophysical Research-Earth Surface*, **113**.

LEE, M. & WAGENMAKERS, E.J. (2014) *Bayesian Cognitive Modeling: A Practical Course*. Cambridge University Press.

MALATESTA, L.C., AVOUAC, J.-P., BROWN, N.D., BREITENBACH, S.F.M., PAN, J., CHEVALIER, M.-L., RHODES, E., SAINT-CARLIER, D., ZHANG, W., CHARREAU, J., LAVÉ, J. & BLARD, P.-H. (2018) Lag and Mixing During Sediment Transfer across the Tian Shan Piedmont Caused by Climate-Driven Aggradation?Incision Cycles Basin Research Early View. *Basin Research***,** n/a

MALATESTA, L.C., PRANCEVIC, J.P. & AVOUAC, J.-P. (2017) Autogenic Entrenchment Patterns and Terraces Due to Coupling with Lateral Erosion in Incising Alluvial Channels. *Journal Of Geophysical Research: Earth Surface*, **122,** 335-355.

MASON, C.C. & ROMANS, B.W. (2018) Climate-Driven Unsteady Denudation and Sediment Flux in a High-Relief Unglaciated Catchment-Fan Using 26al and 10be: Panamint Valley, California *Earth and Planetary Science Letters*.

MCPHILLIPS, D., BIERMAN, P.R., CROCKER, T. & ROOD, D.H. (2013) Landscape Response to Pleistocene-Holocene Precipitation Change in the Western Cordillera, Peru: Be-10 Concentrations in Modern Sediments and Terrace Fills. *Journal of Geophysical Research-Earth Surface*, **118,** 2488-2499.

MEYER-PETER, E. & MULLER, R. (1948) Formulas for Bed-Load Transport. *Proceedings of the 2nd IAHR Meeting, Int. Assoc. of Hydraulic. Eng. and Res. Madrid***,** 39-64.

MICHAEL, N.A., WHITTAKER, A.C. & ALLEN, P.A. (2013) The Functioning of Sediment Routing Systems Using a Mass Balance Approach: Example from the Eocene of the Southern Pyrenees. *Journal of Geology*, **121,** 581-606.

MUELLER, E.R., PITLICK, J. & NELSON, J.M. (2005) Variation in the Reference Shields Stress for Bed Load Transport in Gravel-Bed Streams and Rivers. *Water Resources Research*, **41**.

NICHOLS, K.K., BIERMAN, P.R., CAFFEE, M., FINKEL, R. & LARSEN, J. (2005) Cosmogenically Enabled Sediment Budgeting. *Geology*, **33,** 133-136.

NORTH, F.K. (1985) Exploration Seismology. In: *Petroleum Geology* (Ed. by, 418. Allen and Unwin Inc, Winchester, USA.

PAOLA, C., PARKER, G., SEAL, R., SINHA, S.K., SOUTHARD, J.B. & WILCOCK, P.R. (1992) Downstream Fining by Selective Deposition in a Laboratory Flume. *Science*, **258,** 1757-1760.

PAOLA, C. & SEAL, R. (1995) Grain-Size Patchiness as a Cause of Selective Deposition and Downstream Fining. *Water Resources Research*, **31,** 1395-1407.

PAOLA, C. & MARTIN, J.M. (2012) Mass-Balance Effects in Depositional Systems. *Journal of Sedimentary Research*, **82,** 435-450.

PARKER, G. (1978) Self-Formed Straight Rivers with Equilibrium Banks and Mobile Bed .2. Gravel River. *Journal of Fluid Mechanics*, **89**.

PARKER, G. (1991a) Selective Sorting and Abrasion of River Gravel .2. Applications. *Journal of Hydraulic Engineering-Asce*, **117,** 150-171.

PARKER, G. (1991b) Selective Sorting and Abrasion of River Gravel .2. Applications. *Journal of Hydraulic Engineering*, **117,** 150-171.

PARSONS, A.J., MICHAEL, N.A., WHITTAKER, A.C., DULLER, R.A. & ALLEN, P.A. (2012) Grain-Size Trends Reveal the Late Orogenic Tectonic and Erosional History of the South-Central Pyrenees, Spain. *Journal of the Geological Society*, **169,** 111-114.

PELLETIER, J.D., MURRAY, A.B., PIERCE, J.L., BIERMAN, P.R., BRESHEARS, D.D., CROSBY, B.T., ELLIS, M., FOUFOULA-GEORGIOU, E., HEIMSATH, A.M., HOUSER, C., LANCASTER, N., MARANI, M., MERRITTS, D.J., MOORE, L.J., PEDERSON, J.L., POULOS, M.J., RITTENOUR, T.M., ROWLAND, J.C., RUGGIERO, P., WARD, D.J., WICKERT, A.D. & YAGER, E.M. (2015) Forecasting the Response of Earth's Surface to Future Climatic and Land Use Changes: A Review of Methods and Research Needs. *Earths Future*, **3,** 220-251.

PERUCCA, L.P. & MARTOS, L.M. (2012) Geomorphology, Tectonism and Quaternary Landscape Evolution of the Central Andes of San Juan (30 Degrees S-69 Degrees W), Argentina. *Quaternary International*, **253,** 80-90.

PIZZUTO, J.E. (1995) Downstream Fining in a Network of Gravel-Bedded Rivers. *Water Resources Research*, **31,** 753-759.

RE, G.H., JORDAN, T.E. & KELLEY, S. (2003) Cronologia Y Paleogeografia Del Teriario De La Cuenca Intermontana De Iglesia Septentrional, Andes De San Juan, Argentina. *Revista de la Asociación Geológica Argentina*, **58,** 31-48.

RICE, S. & CHURCH, M. (1996) Sampling Surficial Fluvial Gravels: The Precision of Size Distribution Percentile Estimates. *Journal of Sedimentary Research*, **66,** 654-665.

RICE, S. (1998) Which Tributaries Disrupt Downstream Fining Along Gravel-Bed Rivers? *Geomorphology*, **22,** 39-56.

RICE, S. & CHURCH, M. (1998) Grain Size Along Two Gravel-Bed Rivers: Statistical Variation, Spatial Pattern and Sedimentary Links. *Earth Surface Processes and Landforms*, **23,** 345-363.

RICE, S. (1999) The Nature and Controls on Downstream Fining within Sedimentary Links. *Journal of Sedimentary Research*, **69,** 32-39.

ROBINSON, R.A.J. & SLINGERLAND, R.L. (1998) Grain-Size Trends, Basin Subsidence and Sediment Supply in the Campanian Castlegate Sandstone and Equivalent Conglomerates of Central Utah. *Basin Research*, **10,** 109-127.

RODA-BOLUDA, D.C. & WHITTAKER, A.C. (2018) Normal Fault Evolution and Coupled Landscape Response: Examples from the Southern Apennines, Italy. *Basin Research*, **30,** 186-209.

ROMANS, B.W., CASTELLTORT, S., COVAULT, J.A., FILDANI, A. & WALSH, J.P. (2016) Environmental Signal Propagation in Sedimentary Systems across Timescales. *Earth-Science Reviews*, **153,** 7-29.

RUSKIN, B.G. (2006) Sequence Stratigraphy and Paleopedology of Nonmarine Foreland Basins: Iglesia Basin, Argentina and Axhandle Basin, Utah, Cornell University, NY.

RUSKIN, B.G. & JORDAN, T.E. (2007) Climate Change across Continental Sequence Boundaries: Paleopedology and Lithofacies of Iglesia Basin, Northwestern Argentina. *Journal of Sedimentary Research*, **77,** 661-679.

SEAL, R., PAOLA, C., PARKER, G., SOUTHARD, J.B. & WILCOCK, P.R. (1997) Experiments on Downstream Fining of Gravel .1. Narrow-Channel Runs. *Journal of Hydraulic Engineering-Asce*, **123,** 874-884.

SHIELDS, A. (1936) Awendung Der Aehnlichkeitsmechanik Und Der Turbulenzforschung Auf Die Geschiebebewegung. *MItt. Preuss. Versuchsanst. Wasserbau Schiffau*, **26**.

SIAME, L.L., BOURLES, D.L., SEBRIER, M., BELLIER, O., CASTANO, J.C., ARAUJO, M., PEREZ, M., RAISBECK, G.M. & YIOU, F. (1997) Cosmogenic Dating Ranging from 20 to 700 Ka of a Series of Alluvial Fan Surfaces Affected by the El Tigre Fault, Argentina. *Geology*, **25,** 975-978.

SINGER, M.B. (2008) Downstream Patterns of Bed Material Grain Size in a Large, Lowland Alluvial River Subject to Low Sediment Supply. *Water Resources Research*, **44**.

SNYDER, D.B. (1988) Foreland Crustal Geometries in the Andes of Argentina and the Zagros of Iran from Seismic Reflection and Gravity Data: Phd Thesis, Cornell University, Ithaca, NY.

SURIANO, J., LIMARINO, C.O., TEDESCO, A.M. & ALONSO, M.S. (2015) Sedimentation Model of Piggyback Basins: Cenozoic Examples of San Juan Precordillera, Argentina. *Geodynamic Processes in the Andes of Central Chile and Argentina*, **399,** 221-244.

SYVITSKI, J.P.M. & MILLIMAN, J.D. (2007) Geology, Geography, and Humans Battle for Dominance over the Delivery of Fluvial Sediment to the Coastal Ocean. *Journal of Geology*, **115,** 1-19.

VAL, P., HOKE, G.D., FOSDICK, J.C. & WITTMANN, H. (2016) Reconciling Tectonic Shortening, Sedimentation and Spatial Patterns of Erosion from Be-10 Paleo-Erosion Rates in the Argentine Precordillera. *Earth and Planetary Science Letters*, **450,** 173-185.

VON BLANCKENBURG, F. (2006) The Control Mechanisms of Erosion and Weathering at Basin Scale from Cosmogenic Nuclides in River Sediment (Vol 237, Pg 462, 2005). *Earth and Planetary Science Letters*, **242,** 223-239.

WATERS, J.V., JONES, S.J. & ARMSTRONG, H.A. (2010) Climatic Controls on Late Pleistocene Alluvial Fans, Cyprus. *Geomorphology*, **115,** 228-251.

WHITTAKER, A.C., ATTAL, M. & ALLENN, P.A. (2010) Characterising the Origin, Nature and Fate of Sediment Exported from Catchments Perturbed by Active Tectonics. *Basin Research*, **22,** 809-828.

WHITTAKER, A.C., DULLER, R.A., SPRINGETT, J., SMITHELLS, R.A., WHITCHURCH, A.L. & ALLEN, P.A. (2011) Decoding Downstream Trends in Stratigraphic Grain Size as a Function of Tectonic Subsidence and Sediment Supply. *Geological Society of America Bulletin*, **123,** 1363-1382.

WILCOCK, P.R. & KENWORTHY, S.T. (2002) A Two-Fraction Model for the Transport of Sand/Gravel Mixtures Water Resources Research Volume 38, Issue 10. *Water Resources Research* **38,** 12-11-12-12

WITTMANN, H., VON BLANCKENBURG, F., MAURICE, L., GUYOT, J.L., FILIZOLA, N. & KUBIK, P.W. (2011) Sediment Production and Delivery in the Amazon River Basin Quantified by in Situ-Produced Cosmogenic Nuclides and Recent River Loads. *Geological Society of America Bulletin*, **123,** 934-950.

Appendix

A1. Self-similar grain size distributions and relative mobility function J

Self-similarity among the size distributions of riverbed gravel refers to the scale-invariant shape of their distribution. If the gravel deposits are self-similar, their C_V should to be relatively constant for any downstream distance, where distance is normalized by the length, L, of the depositional system, $x^* = X/L$. In this case, Fedele and Paola (2007) show a similarity variable, ξ, can be derived using:

$$\xi = \frac{D - \overline{D}(x^*)}{\sigma(x^*)} \qquad \textit{Equation A1}$$

where D is the size of each individual grain in a distribution. This self-similar behaviour is predictable through a simplification of the Exner sediment mass balance equation for when the Shields parameter, i.e. the non-dimensionalized critical shear stress required for particle entrainment, is cross-sectionally averaged. In this case, sediment transport and deposition, typically described by Hirano's three layer sediment sorting model (Hirano, 1971), can be expressed as a simple, probabilistic partitioning ratio between the size fraction of clasts in transport, p_i, and the size fraction on the bed surface, $F_{\cdot i}$.

$$J_i = p_i / F_{\cdot i} \qquad \textit{Equation A2}$$

where the mobility function, J_i, describes the relative mobility of clast sizes deposited locally (Fedele & Paola, 2007; Duller *et al.*, 2010). Assuming both the bed surface size distributions and the form of the relative mobility function, J, can be collapsed into the same similarity solution, the bed surface size distribution can be used to reconstruct J.

Fedele and Paola (2007) derive a function for J using a semi-empirical, hydraulically based fining model, ACRONYM, calibrated against field and experimental data (Parker, 1991b) and based on their transformation of the measured grain size distributions into self-similar ξ distributions. They parameterize the relative mobility function J as:

$$J_i = a_g e^{-b_g \xi} + c_g \qquad \text{Equation A3}$$

where a_g, b_g and c_g are constants that characterise the incipient motion of gravel. Sediment entrainment is considered dependent solely on particle size; therefore, a_g scales with the mobility of all clast sizes, b_g describes the rate at which clasts of increasing size become less mobile than smaller clasts, and c_g relates to the minimum probability of entraining a clast of any size. The shape and structure of the relative mobility function *J* is expected to depend on the nature of the transport

regime; the formulation above is for sediments coarser than sand (Whittaker *et al.*, 2011; D'Arcy *et al.*, 2017), for which bed load transport is likely to be the dominant mode.

A2. Impact of abrasion on downstream grain size fining in the Iglesia basin

The breakdown of clasts during sediment transport is dependent on the resistance of clasts to abrasion and the distance over which the clasts have been transported (Attal & Lavé, 2009). Abrasion should contribute to downstream fining on alluvial fan, and we assess its relative contribution to the fining trends by observing how the proportions of clast lithologies in our samples change downstream.

We sampled the lithology and size of 200 clasts at each sample location using a Wolman point count technique for clast selection, i.e., clasts were selected randomly from a predefined area ~ $2m^2$. The b-axis of each clast was measured and its lithology categorised as Intrusive, Extrusive, Sedimentary, Metamorphic or Quartzite. In figure A1, the proportions of the different lithologies present at each site are plotted against their distance downstream, from fan apex to toe.

Intrusive and extrusive rocks are expected to abrade at a low rate, typically less than 1 % mass loss / km, equivalent to a downstream fining rate of 0.3 % / km (Attal *et al.*, 2006; Attal & Lavé, 2009). However, the abrasion rate of sedimentary rocks, which make up to half of the gravel on the fans, is more difficult to constrain. If sedimentary rocks were abraded faster than the other rocks, then we would expect a systematic downstream decrease in the relative proportion of sedimentary gravel with respect to the other rock types. We observe no systematic change in the relative proportion of lithologies across fans 2 and 3, suggesting no preferential abrasion of any particular lithology on these fans (figure A1). We can therefore assume that all gravel is as resistant, with an abrasion rate unlikely to exceed 1 % mass loss / km, and therefore a minimal contribution to the observed downstream fining at rates of 6.7 and 5.9 % / km on fans 2 and 3, respectively.

On fan 1 however, we note that the contribution of gravel from sedimentary rocks gradually decreases from ~50 % of all gravel at the apex of the fan to ~30 % at a distance of nearly 40 km downstream, while the relative proportion of extrusive gravel and quartzite increases (figure A1). This suggests that the gravel made of sedimentary rocks is abraded faster than the others, and that abrasion may therefore contribute to the observed downstream fining on the fan. To assess the magnitude of the phenomena, we run a very simple model of gravel abrasion that predicts the evolution of a mixture made of hard and soft gravel abrading at two different rates (Supplementary Information). We find that if the hard rocks are abrading at a conservative rate of 1 % mass loss / km, then the soft gravel needs to abrade at a rate of 3.1 % / km to have its contribution reduced from 50 to 30 % over a distance

of 40 km. The equivalent mass loss rate for the mixture is 1.9 % / km, equivalent to a fining rate of 0.6 % / km (Supplementary Information). Because the fining rate observed on fan 1 is 1.8 % / km, we conclude that abrasion may contribute up to 30 % of the observed fining rate. We note that this is a conservative estimate: we used a mass loss rate for the hard rock of 1 % / km but most of the change in relative lithological proportions observed is driven by quartzite, which tends to abrade at a much lower rate, typically 0.1-0.2 % / km.

A3. Varying basin subsidence

In figure A2, alongside the measured grain size fining trends, we present modelled downstream grain size fining trends for a range of other subsidence profiles that have no physical constraint other than their wavelength, which is set by the width of the basin. Without prior constraint on the profile of basin subsidence, the data can be fitted using the single source model with an exponential subsidence profile typical of a normal-fault-bounded basin. This predicted profile is the inverse of the basin structure that we measure. Fan 2 is fitted well by a subsidence profile with an exponent of 0.05 m/ x*, which yields a maximum subsidence rate of 1.7 m/10kyr. Fining profiles on fans 1 and 3 are less well fitted by this profile of subsidence and this is due to the fact that relatively coarse gravel is still found up to the toe of these fans; a characteristic that is difficult to resolve with a model solution that assumes 100% of gravel sizes are exhausted at the maximum downstream length. This experiment highlights the uncertainty in fitting self-similar grain size fining models to field data.

A4. Tributary Inputs

	Non-linear least squares regression	68% (σ) confidence	95% (2σ) confidence	RMSE	p -value for α	$\widehat{l_1}$
Fan 1	$D_0 = 93\,mm$ $\alpha = -0.018$/ km	$D_0 = 88\,mm$ $\alpha = -0.022$/ km $D_0 = 99\,mm$ $\alpha = -0.014$/ km	$D_0 = 79\,mm$ $\alpha = -0.028$/ km $D_0 = 107\,mm$ $\alpha = -0.009$/ km	12.07	0.006	7.29
Fan 2	$D_0 = 164\,mm$ $\alpha = -0.067$/ km	$D_0 = 145\,mm$ $\alpha = -0.081$/ km $D_0 = 182\,mm$ $\alpha = -0.054$/ km	$D_0 = 122\,mm$ $\alpha = -0.099$/ km $D_0 = 205\,mm\ \alpha = -0.037$/ km	23.02	0.019	8.35
Fan 3	$D_0 = 119\,mm$ $\alpha = -0.059$/ km	$D_0 =$114 mm $\alpha = -0.061$/ km $D_0 =$ 123 $mm\ \alpha = -0.052$/ km	$D_0 = 106\,mm$ $\alpha = -0.069$ / km $D_0 = 130\,mm\ \alpha = -0.045$ / km	7.169	0.001	6.02

Table 1: Empirical model fit to data. The expoential relation that attains a log-llikelihood function, $\widehat{l_1}$, with the lowest residual sum of squares is reported as the intercept grain size, D_0, and the downstream fining exponent α, for each respective fan. We quote the Root Mean Square Error (RMSE) and the p-value for the fining exponent, α. The table includes the 68 and 95 % confidence intervals on this empirical best fit to the data.

	Fan 1		Fan 2		Fan 3	
	x*	% q_s	x*	% q_s	x*	% q_s
Primary catchment	0	54	0	82	0	32
Tributary catchments	0.17	16	0.54	1	0.31	15
	0.33	1	0.58	17	0.38	6
	0.36	2			0.42	47
	0.38	27				

Table A1: Percentage of the total sediment flux, $\% q_s$, supplied by each catchment at the normalised downstream distance, x^*, along the trunk stream. Each catchment is delineated in igure 1. Sediment fluxes were estimated using the BQART sediment flux model after Syvitski and Milliman (2007) (Harries et al., 2018). Tributary confluences were mapped from satellite imagery.

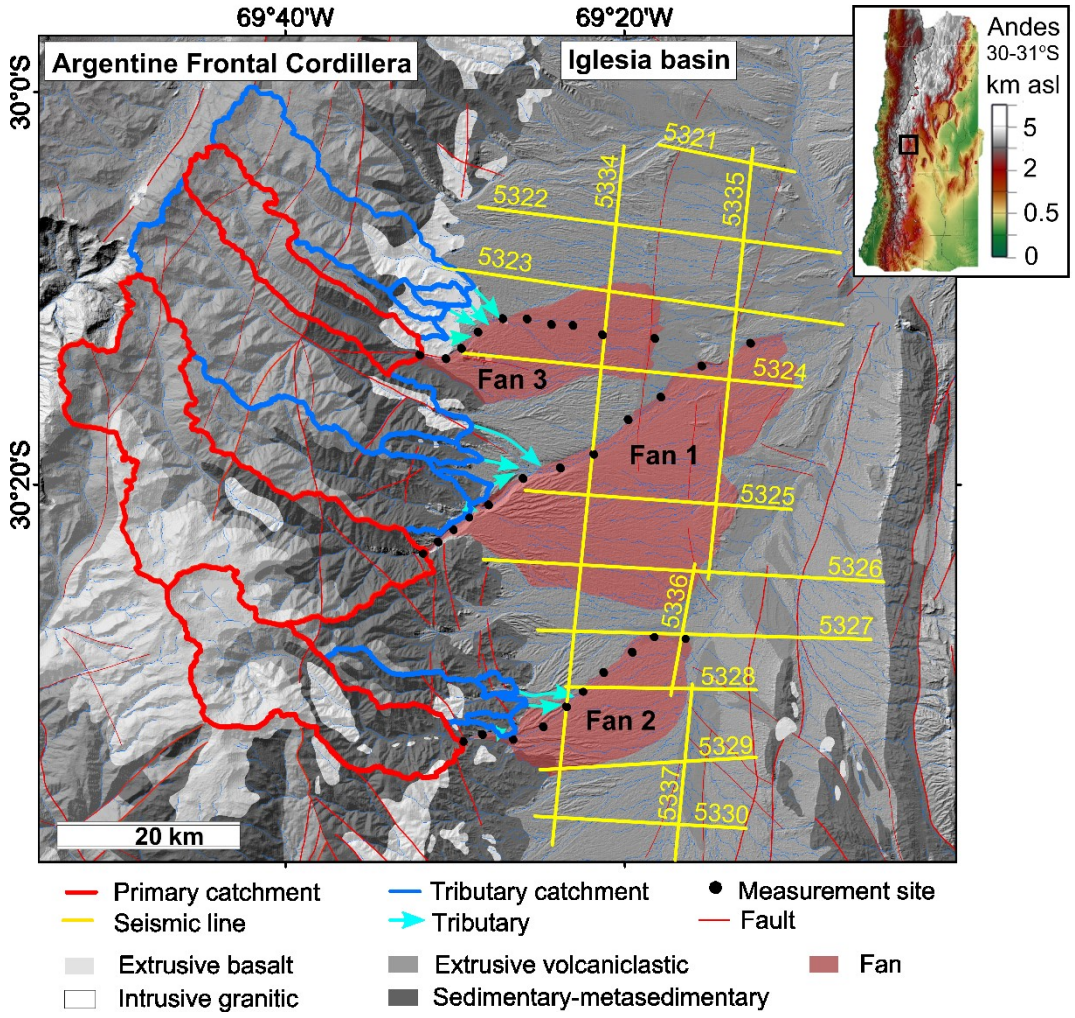

Figure 1: The Iglesia basin catchment-alluvial fans. Bedrock lithology and faults are taken from geological maps produced by the Argentine Servicio Geologico Minero (SEGEMAR). Seismic survey lines are taken from Ruskin (2006) and Beer (1990). There are ten west-east profiles ~25-35 km in length and four north-south tie lines, between 15 and 75 km in length. The top right inset is an ETOPO1 relief model, downloaded from the NCEI database (Amante & Eakins, 2009) which highlights the location of the Iglesia basin in the eastern foreland of the Andean mountain chain, 30-31^{0}S. Photographs show tributaries and incised fan surfaces are important geomorphic features on these large alluvial piedmonts.

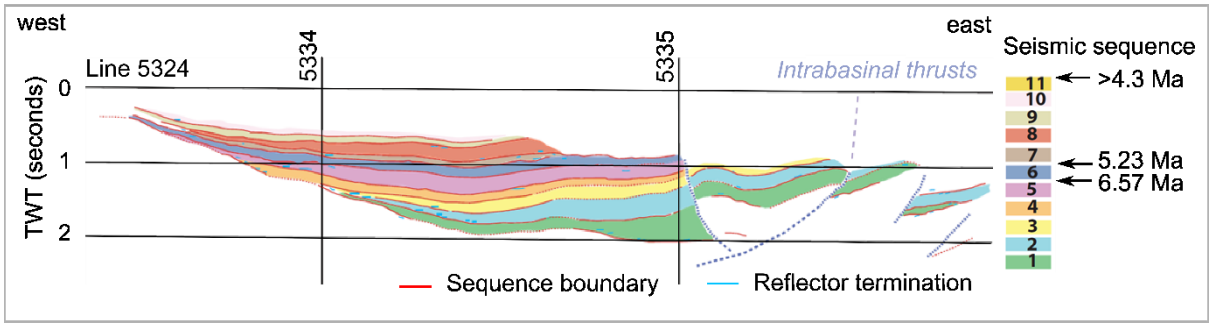

Figure 2: Interpretation of seismic data collected close to the basin axis, along line 5324, adapted from Ruskin (2006)

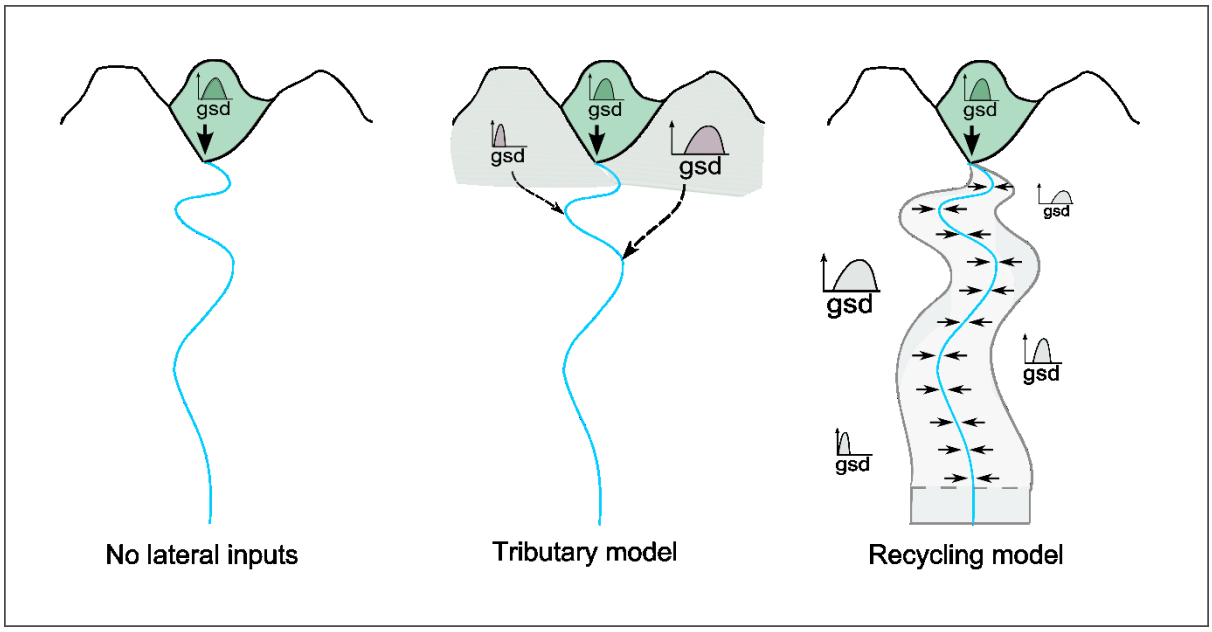

Figure 3: Idealised end-member models for sediment sourcing on alluvial piedmonts. The no lateral inputs model, or single input model, is typically used in sediment routing system modelling. The tributary model illustrates the lateral incorporation of sediment from additional point sources with potentially very different grain size distributions to the trunk stream (gsd). The recycling model captures the lateral incorporation of sediment by older fan surface reworking. The sediment is supplied along the length of the depositional system and the grain size distributions of recycled fan material are likely spatially variable. Within the self-similar model, the flux and grain size of the sediment supplies are free parameters, though within each iteration we keep the gsd of all inputs the same in order to reduce complexity.

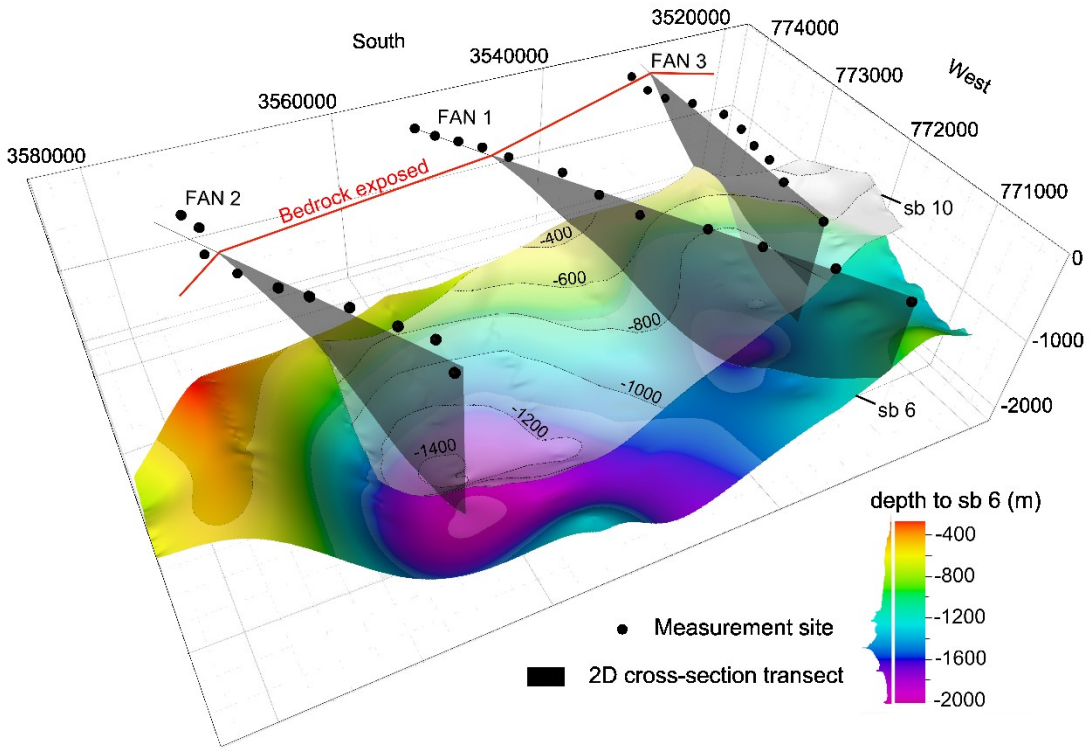

Figure 4: 3D model of the stratigraphy of the Iglesia basin. The isopachs of two sequence boundaries are plotted. The oldest boundary, sb6, is the coloured surface where the isopach depth is given in the legend alongside its hypsometric depth distribution. The youngest boundary with good spatial coverage, sb10 is plotted in white and has isopach depth contours. Black dots highlight the locations at the surface of the Earth where grain size measurements were taken for each fan and the red line delineates where bedrock is exposed. Depth slices outline the transect along which 2D subsidence profiles were extracted for each fan.

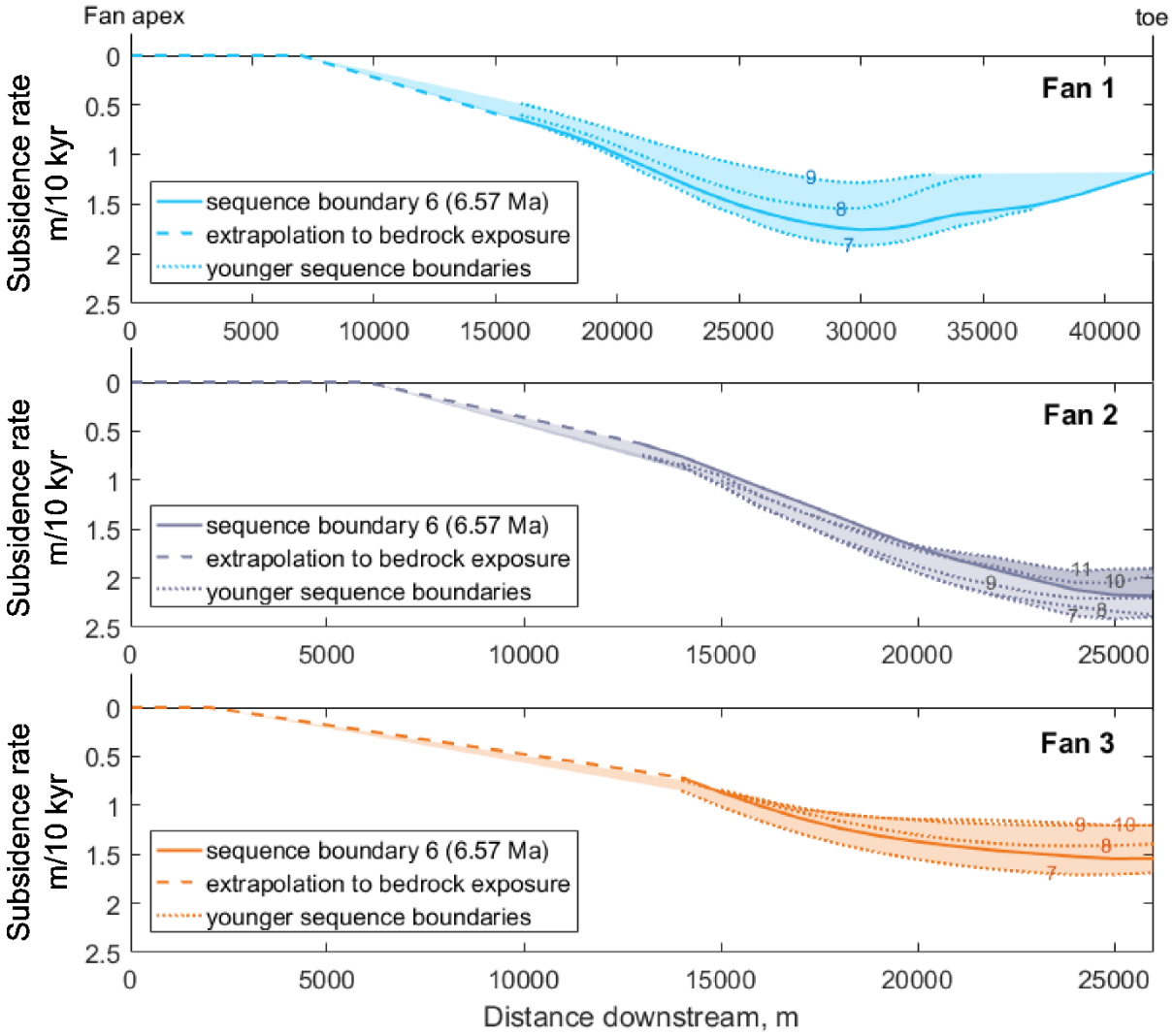

Figure 5: Spatial distribution of differential subsidence along 2D transects highlighted in figure 4. Transects are taken from the fan apex to toe and are plotted as downstream distance from the fan apex. The sequence boundary cross-sections are numbered and correspond with respective isopach maps in appendix figure A1. For fan 3, sb11 is not well imaged; similarly, for fan 1, sb 10 and 11 are only partially imaged and are therefore omitted from the analysis. The younger sequences are poorly imaged or discontinuous in the west of the basin, which results in an apparent overlapping of sb 10 and 11 for fan 2 and sb 9 and 10 for fan 3, where boundaries have been extrapolated toward the mountain front tracing the sb below. Sequence boundary 6 is used to constrain subsidence in the self-similar fining model as this is the most continuous sequence boundary mapped.

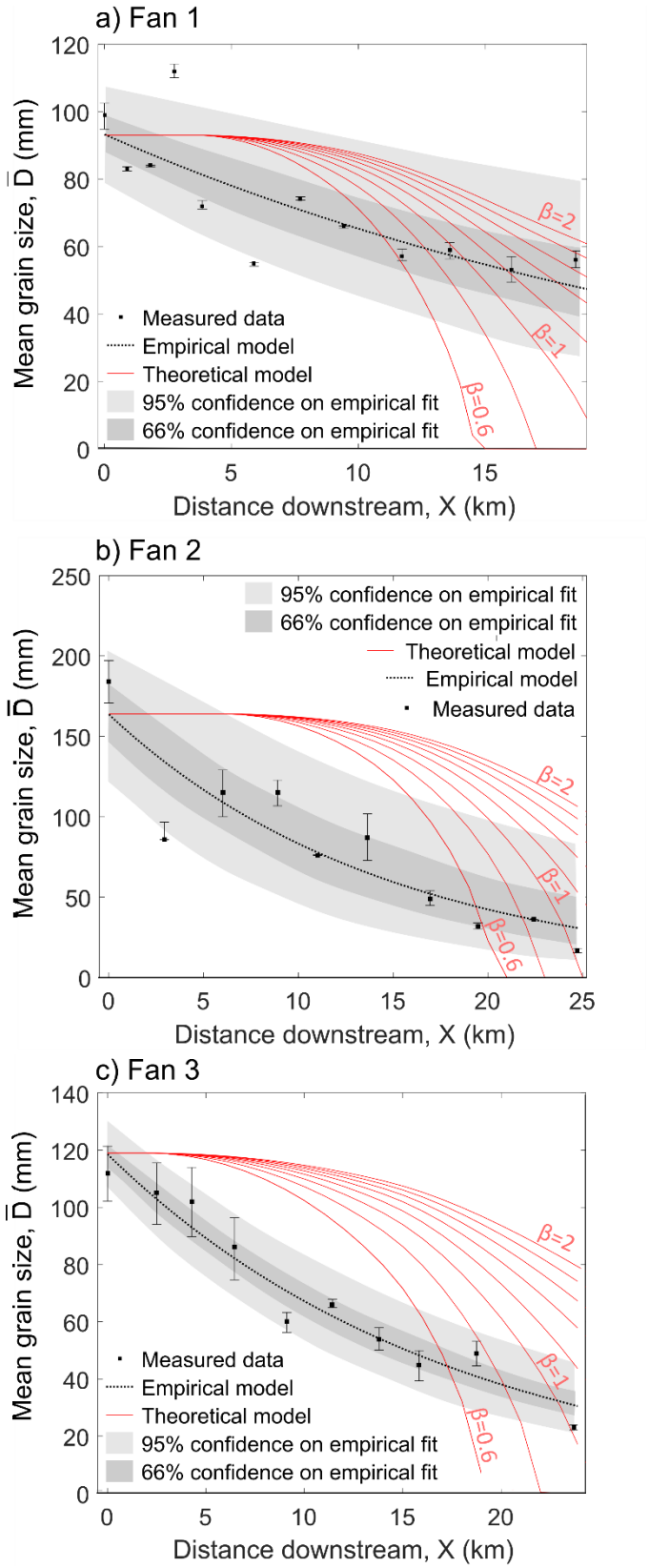

1144

1145 *Figure 6: Single input model solutions for a range of basin fill fractions, β.*

1146

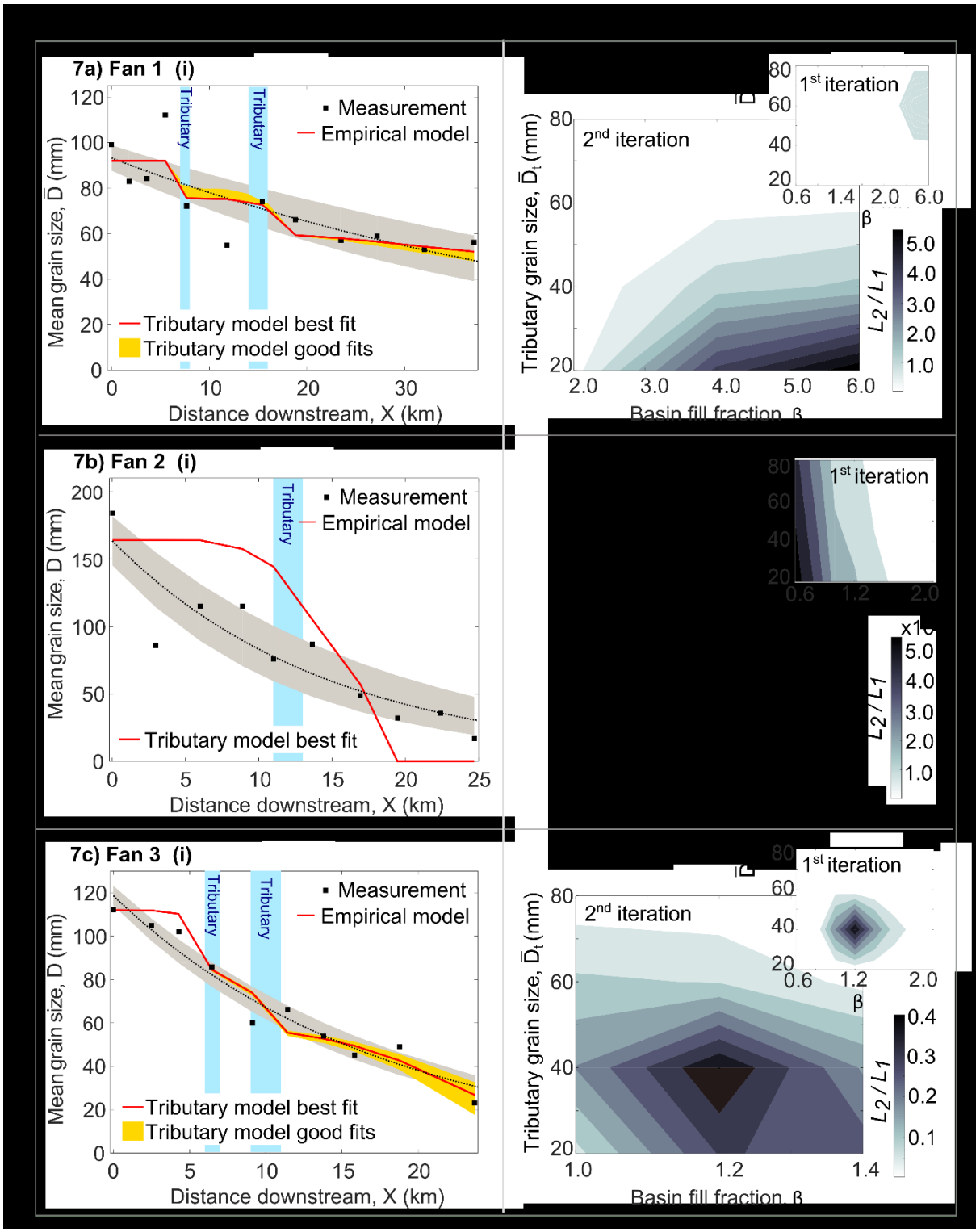

Figure 7: (i) Best fit and good fit tributary model solutions for grain size data on each fan. (ii) Isopachs of the likelihood ratio calculated for each model solution. For the first iteration, all tributary inputs have the same input grain size D_t. On the second iteration, the grain size of the lower fan tributaries is fixed at the best fit solution from the first iteration and the grain size of the upper fan tributaries is varied independently. A second iteration was not performed for fan 2 as the first iteration failed to find a good fit to the data.

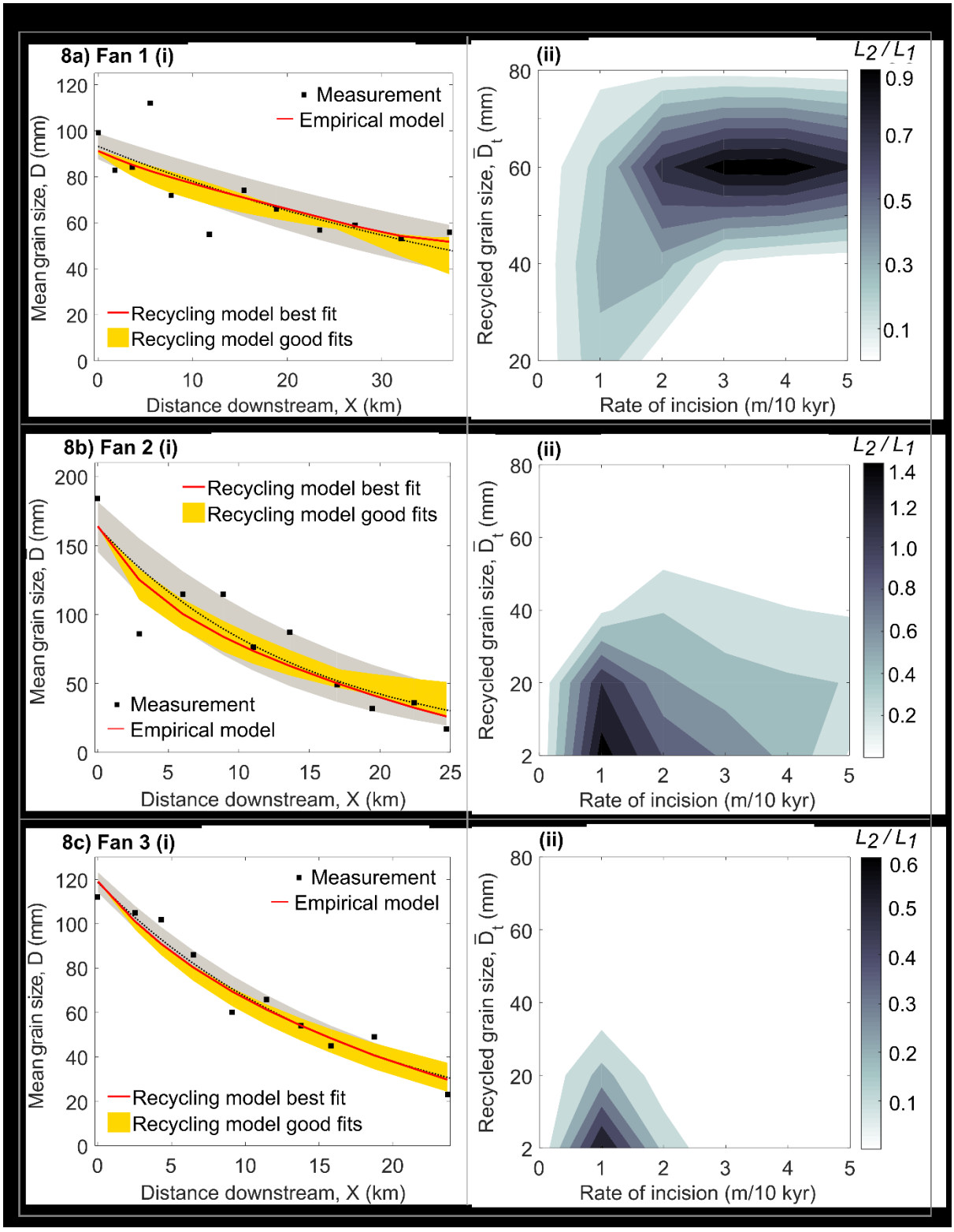

Figure 8: (i) Best fit and good fit recycled model solutions for grain size data on each fan. (ii) Isopaches of the likelihood ratio calculated for each model solution.

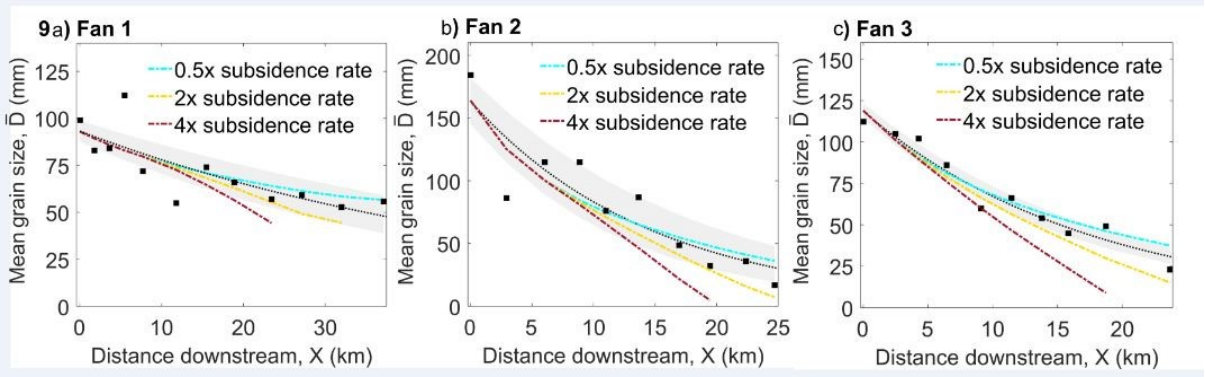

1159

1160

1161 *Summary figure 9: (a-c) Change in grain size fining profile of the best fit recycling model solution in response to*
1162 *a change in the rate of basin subsidence.*

1163

1164

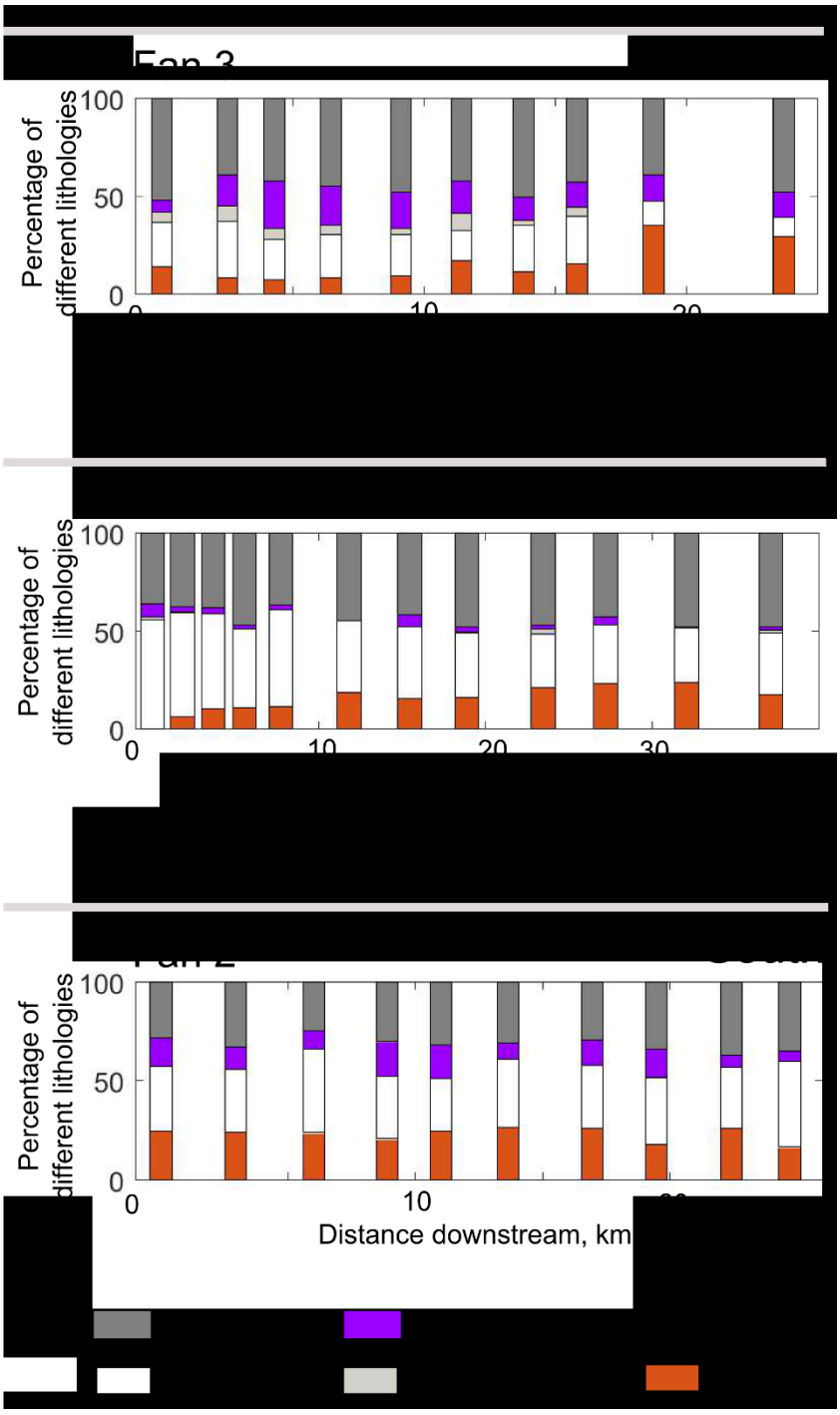

Figure A1: The proportions of different lithologies sampled at each site along the length of each fan.

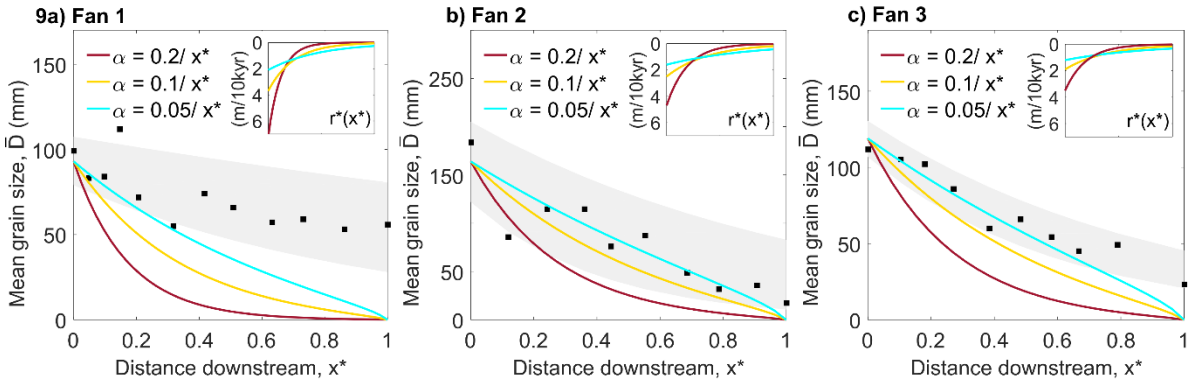

1170

1171

1172 *Figure A2: Range of grain size fining model solutions attained for when the spatial distribution of tectonic*
1173 *subsidence, r*(x*), is only constrained by the maximum width of the basin, by first order sediment flux*
1174 *estimations from the BQART model and an assumption that the basin is 100 % filled. The exponent of r*(x*) is*
1175 *varied between α = 0.2 and α = 0.05 to attain a fit to the data. The grey band is the 95% confidence interval for*
1176 *the fit of the empirical exponential to the measured data. The graphical insets plot the profiles of subsidence for*
1177 *when the exponent of r*(x*) is set to 0.2, 0.1 and 0.05, respectively.*

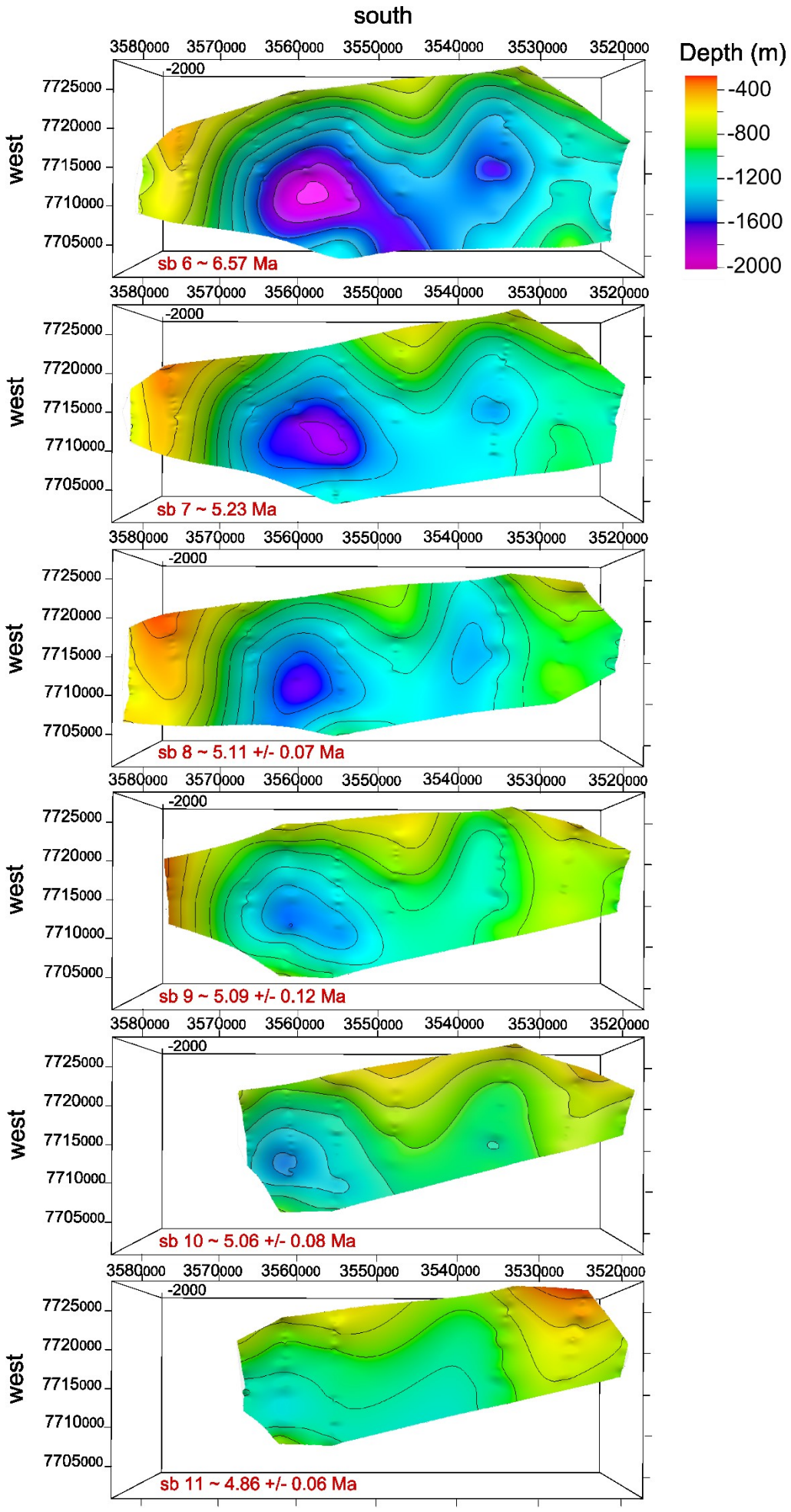
south
west
3580000 3570000 3560000 3550000 3540000 3530000 3520000
7725000
7720000
7715000
7710000
7705000
-2000
Depth (m)
-400
-800
-1200
-1600
-2000
sb 6 ~ 6.57 Ma
sb 7 ~ 5.23 Ma
sb 8 ~ 5.11 +/- 0.07 Ma
sb 9 ~ 5.09 +/- 0.12 Ma
sb 10 ~ 5.06 +/- 0.08 Ma
sb 11 ~ 4.86 +/- 0.06 Ma

Figure A3: Isopach maps of sequence boundaries 6 to 11 constructed in Petrel™ using 2D seismic interpretations of basin fill previously published in Ruskin (2006). Sequence boundaries (sb) 6 and 7 have previously established age constraints (section 3.2) and sb 11 is given a minimum age of deposition of > 4.3 Ma. The ages of sb's 8-11 are estimated using rates of sediment accumulation at the average depth interval between sb 7 and sb 11, with the spatial variation in accumulation rate given as a plus or minus error.